

NUMERICAL COMPUTATIONS OF GEOMETRIC ERGODICITY FOR STOCHASTIC DYNAMICS

YAO LI AND SHIROU WANG

ABSTRACT. A probabilistic approach of computing geometric rate of convergence of stochastic processes is introduced in this paper. The goal is to quantitatively compute both upper and lower bounds of the exponential rate of convergence to the invariant probability measure of a stochastic process. By applying the coupling method, we derive an algorithm which does not need to discretize the state space. In this way, our approach works well for many high-dimensional examples. We apply this algorithm to both random perturbed iterative mappings and stochastic differential equations. We show that the rate of geometric ergodicity of the random perturbed system can, to some extent, reveal the chaotic properties of the unperturbed deterministic one. Various SDE models including those with degenerate noise or high-dimensional state space are also explored.

1. INTRODUCTION

In this paper, we consider stochastic processes arising from random perturbed deterministic dynamical systems. The dynamics of such a stochastic process, say $\mathbf{X} = \{X_t; t \in \mathbb{R}\}$, is a combination of the random perturbation and the underlying deterministic dynamics. The ergodicity of \mathbf{X} , and the rate of ergodicity, i.e., the speed of convergence of the law of X_t to its invariant probability measure, is a significant quantity given by the spectral gap of the infinitesimal generator of \mathbf{X} . From an applied point of view, knowing the speed of convergence is very useful to sampling, uncertainty quantification, and sensitivity analysis [12, 24, 37].

However, the ergodicity of a stochastic process is difficult to study in a quantitative way. The spectral method, which tries to estimate the spectral gap directly, only works for a limited class of problems such as over-damped Langevin dynamics [2, 30]. The probabilistic approach, on the other hand, although being “softer” and more applicable, usually does not give a precise bound in most of existing results. For instance, by constructing a Lyapunov function and showing the minorization condition of a certain “small set”, one can easily deduce the geometric ergodicity [18, 19, 36]. Nevertheless, the rate of geometric ergodicity obtained in this way is far from being optimal. In most cases, we only know that the speed of convergence to steady state is approximately being ρ^t for some $\rho < 1$, but ρ is usually too close to 1 to be useful in practice.

Key words and phrases. Stochastic process, Stochastic Differential Equations, Geometric ergodicity, coupling method.

Y. L. is partially supported by NSF DMS-1813246. S. W. was partially supported by NSFC grants 11771026, 11471344, and acknowledges PIMS-CANSSI postdoctoral fellowship.

The computational study of the ergodicity, on the other hand, is far from being mature. While one can compute eigenvalues of the discretized infinitesimal generator for low-dimensional problems (1D or 2D) just as discussed in [22], this approach does not work well if \mathbf{X} lives in a higher dimensional space. One can also obtain the convergence rate by computing the correlation decay of a test function using the Monte Carlo simulation. However, as discussed in [31], the correlation (or auto-correlation) has small expectation and large variance, which results in an unrealistic requirement of large amount of samples in real simulations. In addition, the selection of test functions is very subjective.

The main goal of this paper is to propose a coupling approach, a powerful tool that has been used in many rigorous and computational studies [5, 16, 23, 34, 35], to numerically compute the geometric ergodicity. Traditionally, coupling method is mainly used in the theoretical study of stochastic dynamics. This is partially because for stochastic differential equations, a numerically simulated trajectory only approximate the real trajectory at discrete times with certain accuracy. As a result, on a continuous state space, two numerical trajectories can easily “miss” each other even if the actual trajectory have been coupled together. We solve this problem by using the maximal coupling whenever two trajectories are sufficiently close to each other, and develop a numerical coupling scheme. By applying to various examples, we show that our numerical coupling algorithm works well for iterative mappings with random perturbations, stochastic differential equations with non-degenerate diffusion, as well as high-dimensional oscillators. Also, it can be adapted for certain systems with degenerate diffusion with some extra computational cost.

A secondary goal of our study is to reveal the dependence of geometric ergodicity of the perturbed stochastic systems on the underlying deterministic dynamics. By applying on random perturbed circle maps with distinct chaotic behaviors, our result shows that the rate of geometric ergodicity, or heuristically the spectral property, can reveal, in some sense, the mixing property of the underlying dynamics. For example, when the magnitude of noise decreases, the rate of geometric ergodicity drops “quickly” when the underlying dynamics is ergodic but not mixing (quasi-periodic orbits), while the rate drops “dramatically” when the underlying dynamics admits a stable periodic orbit (See Section 4 for more details). Our simulation also shows that larger time scale separation between slow and fast deterministic dynamics can increase, when random noise is added, the rate of geometric convergence to the invariant probability distribution of the stochastic dynamics. This is consistent with the heuristic argument.

The paper is organized as follows. Section 2 gives necessary probability and dynamical system preliminaries for our study. Our numerical algorithms are described in Section 3. Section 4 studies the connection of geometric ergodicity with the chaotic properties of the deterministic dynamics by several examples of iterative mappings with distinct mixing properties on circle. Examples of stochastic differential equations with various deterministic or random structures are studied in Section 5. We make conclusion and further discussions in Section 6.

2. PROBABILITY AND DYNAMICAL SYSTEMS PRELIMINARY

2.1. **Markov process and geometric ergodicity.** Let E be a state space, which can be $\mathbb{R}^k, \mathbb{T}^k$, or a subset of \mathbb{R}^k , with σ -field \mathcal{B} . Consider a Markov process $\mathbf{X} = \{X_t; t \in \mathcal{T}\}$ on (E, \mathcal{B}) , where \mathcal{T} can be $\mathbb{R}_{\geq 0}, \mathbb{Z}_{\geq 0}$, or $h\mathbb{Z}_{\geq 0} := \{0, h, 2h, \dots\}$ for $h > 0$, with transition probabilities $\mathcal{P} = \{P^t(x, \cdot); t \in \mathcal{T}\}$, i.e., for any $t \in \mathcal{T}$, $P^t(\cdot, A)$ is a measurable function for each fixed $A \in \mathcal{B}$, and $P^t(x, \cdot)$ is a probability measure for each fixed $x \in E$ such that

$$P^t(x, \cdot) = \int_E P^s(x, dy) P^{t-s}(y, \cdot), \quad 0 \leq s \leq t.$$

For a reference measure ϕ on (E, \mathcal{B}) , \mathbf{X} is said to be ϕ -irreducible if for any $x \in E$, $\phi(A) > 0$ implies that $P^t(x, A) > 0$ for some $t > 0$.

For any probability measure μ on (E, \mathcal{B}) , the evolution of μ is denoted as

$$\mu P^t(\cdot) := \int_E P^t(x, \cdot) \mu(dx), \quad t \in \mathcal{T}.$$

A measure π is called invariant if $\pi P^t = \pi$ holds for any t . A Markov process \mathbf{X} is said to be *ergodic* if it admits a unique invariant probability measure π such that for any $x \in E$, $\lim_{t \rightarrow \infty} \delta_x P^t = \pi$. Throughout this paper, we assume that the Markov process \mathbf{X} is ergodic with an invariant probability measure π . It is not hard to see that \mathbf{X} is π -irreducible.

The emphasis of this paper is the geometric ergodicity. An ergodic Markov process \mathbf{X} is said to be *geometrically ergodic* with rate $r > 0$ if for π -a.e. $x \in E$,

$$\limsup_{t \rightarrow \infty} \frac{1}{t} \log(\|\delta_x P^t - \pi\|_{TV}) = -r,$$

where $\|\cdot\|_{TV}$ is the total variation distance, i.e., $\|\mu - \nu\|_{TV} = \sup_{A \in \mathcal{B}} |\mu(A) - \nu(A)|$. We say that \mathbf{X} is *geometrically contracting* with rate $r > 0$ if for $\pi \times \pi$ -almost every initial pairs (x, y) , it holds that

$$\limsup_{t \rightarrow \infty} \frac{1}{t} \log(\|\delta_x P^t - \delta_y P^t\|_{TV}) = -r.$$

Note that by the triangular inequality, geometric ergodicity implies the geometric contraction.

2.2. **Coupling of Markov processes.** Let μ and ν be two probability measures on (E, \mathcal{B}) . A *coupling* between μ and ν is a probability measure on $E \times E$ whose first and second marginals are respective μ and ν . For random variables X and Y taking values in E with respective distribution μ and ν , we have the following well-known inequality (see, e.g., Lemma 3.6. in [1])

$$(2.1) \quad \|\mu - \nu\|_{TV} \leq 2\mathbb{P}[X \neq Y]$$

In the present paper, we consider the coupling of Markov processes. Given Markov processes $\mathbf{X} = \{X_t; t \in \mathcal{T}\}$ and $\mathbf{Y} = \{Y_t; t \in \mathcal{T}\}$ on (E, \mathcal{B}) sharing the same transition probabilities $\mathcal{P} = \{P^t(x, \cdot); t \in \mathcal{T}\}$. A *coupling* of \mathbf{X} and \mathbf{Y} is a stochastic process $(\mathbf{X}, \mathbf{Y}) = \{(\mathcal{X}_t, \mathcal{Y}_t); t \in \mathcal{T}\}$ on $E \times E$ such that

- (i) The first and second marginal processes $\{\mathcal{X}_t\}$ and $\{\mathcal{Y}_t\}$ are respective copies of \mathbf{X} and \mathbf{Y} ;
- (ii) If $s \in \mathcal{T}$ be such that $\mathcal{X}_s = \mathcal{Y}_s$, then $\mathcal{X}_t = \mathcal{Y}_t$ for all $t > s$.

The first meeting time of \mathcal{X}_t and \mathcal{Y}_t , denoted as $\tau_c := \inf_{t \geq 0} \{\mathcal{X}_t = \mathcal{Y}_t\}$, is called the *coupling time*. The coupling (\mathbf{X}, \mathbf{Y}) is said to be successful if the coupling time is almost surely finite, i.e., $\mathbb{P}[\tau_c < \infty] = 1$.

Lemma 2.1. *Let (\mathbf{X}, \mathbf{Y}) be a coupling of a Markov process (admitting transition probabilities $\mathcal{P} = \{P^t(x, \cdot); t \in \mathcal{T}\}$) with initial distribution $\mu \times \nu$. Then*

$$(2.2) \quad \|\mu P^t - \nu P^t\|_{TV} \leq 2\mathbb{P}[\tau_c > t].$$

Proof. By the definition of coupling time, $\mathcal{X}_t \neq \mathcal{Y}_t$ implies that $\tau_c > t$. By noting that μP^t (resp. νP^t) is the distribution of \mathcal{X}_t (resp. \mathcal{Y}_t), it follows from (2.1) that

$$\|\mu P^t - \nu P^t\|_{TV} \leq 2\mathbb{P}[\mathcal{X}_t \neq \mathcal{Y}_t] \leq 2\mathbb{P}[\tau_c > t].$$

□

We call (2.2) the *coupling inequality*. A coupling (\mathbf{X}, \mathbf{Y}) is said to be an *optimal coupling* if the equality in (2.2) is achieved. Besides, a coupling (\mathbf{X}, \mathbf{Y}) is said to be a *Markov coupling* if (\mathbf{X}, \mathbf{Y}) is a Markov process on $E \times E$. A Markov coupling (\mathbf{X}, \mathbf{Y}) is further called *irreducible* if it is $\pi \times \pi$ -irreducible, where π is the unique invariant probability measure of \mathbf{X} and \mathbf{Y} .

In the present paper, we estimate the rate of geometric ergodicity from below via (2.2). However, in practice, we cannot compute the coupling time for all initial values. Therefore, some theoretical arguments are necessary to extend the result from one initial value to almost all initial values. The following lemma plays a such role that enable us to extend the finiteness of moment generating function of the coupling time from one pair of initial values to $\pi \times \pi$ -almost every pairs of initial values.

Lemma 2.2. *Assume (\mathbf{X}, \mathbf{Y}) is an irreducible Markov coupling. If there exists a pair of initial value $(x_0, y_0) \in E \times E$ and a constant $r_0 > 0$ such that*

$$(2.3) \quad \mathbb{E}_{(x_0, y_0)}[e^{r_0 \tau_c}] < \infty,$$

then (2.3) holds for $(\pi \times \pi)$ -a.e. pair of initial values.

Proof. Suppose that the proposition does not hold, then there exists a measurable set $A \subseteq E \times E \setminus \{(x, x) : x \in E\}$ with $(\pi \times \pi)(A) > 0$ such that

$$(2.4) \quad \mathbb{E}_{(x, y)}[e^{r_0 \tau_c}] = \infty$$

holds for any pair $(x, y) \in A$.

By irreducibility, there exists $T > 0$ such that $\mathbb{P}_{(x_0, y_0)}[(\mathcal{X}_T, \mathcal{Y}_T) \in A] > 0$. Then by (2.4) and the Markov property, we have

$$\mathbb{E}_{(x_0, y_0)}[e^{r_0 \tau_c}] \geq \mathbb{P}_{(x_0, y_0)}[(\mathcal{X}_T, \mathcal{Y}_T) \in A] \cdot \mathbb{E}_\mu[e^{r_0 \tau_c}] = \infty,$$

where μ is the conditional probability measure of (\mathbf{X}, \mathbf{Y}) conditioning on $(\mathcal{X}_T, \mathcal{Y}_T) \in A$. This contradicts with (2.3). □

One problem with Lemma 2.2 is that many efficient couplings we shall use, such as the reflection coupling introduced in Section 3, are not irreducible. On the other hand, although the independent coupling (i.e., the two marginal processes are updated independently all the time) brings about the irreducibility, it is usually not efficient for the coupling process. In fact, most stochastic processes in \mathbb{R}^k (e.g., a strong-Feller process), including all the numerical examples in this paper, are *non-atomic*, which means that any two independent trajectories of \mathbf{X} , say X_t^1 and X_t^2 , satisfy $\mathbb{P}[X_{t+1}^1 = X_{t+1}^2 \mid X_t^1 \neq X_t^2] = 0$. (Without loss of generality, we assume that $\mathcal{T} = \mathbb{Z}_{\geq 0}$.) So independent coupling of a non-atomic Markov process has zero probability of being coupled successfully in finite time.

To overcome this difficulty, we introduce the coupling with independent components. Still, without loss of generality, we assume $\mathcal{T} = \mathbb{Z}_{\geq 0}$. A *coupling with independent components* means that at each step before coupled, there is a positive probability (can be very small) that the two marginal processes are updated in an independent way. The following lemma shows that a coupling with independent components of a non-atomic Markov process is irreducible. In this way, we can use a mixture of independent coupling and other more efficient couplings to achieve both the irreducibility and the coupling efficiency.

Lemma 2.3. *Assume (\mathbf{X}, \mathbf{Y}) is a coupling with independent components of a non-atomic Markov process. Then (\mathbf{X}, \mathbf{Y}) is $\pi \times \pi$ -irreducible.*

Proof. It is sufficient to show that for any product set $A_1 \times A_2 \in \mathcal{B} \times \mathcal{B}$ with positive $\pi \times \pi$ measure, there exists some $t_0 \in \mathcal{T}$ such that $\mathbb{P}[(\mathcal{X}_{t_0}, \mathcal{Y}_{t_0}) \in A_1 \times A_2] > 0$.

By the ergodicity, since $A_1 \in \mathcal{B}$ has positive π -measure, there exists $T_1 > 0$ such that $\mathbb{P}[X_t \in A_1] > 0$ for all $t > T_1$. Similarly, there exists $T_2 > 0$ such that $\mathbb{P}[Y_t \in A_2] > 0$ for all $t > T_2$. Let $t_0 = \max\{T_1, T_2\} + 1$. Because there is a positive probability that independent updates be chosen for $t = 0, 1, \dots, t_0$, and the Markov process is non-atomic, we have $\mathbb{P}[(\mathcal{X}_{t_0}, \mathcal{Y}_{t_0}) \in A_1 \times A_2] > 0$. □

Lemma 2.4. *Assume (\mathbf{X}, \mathbf{Y}) is a coupling with independent components of a non-atomic Markov process. If there exists an initial value $x_0 \in E$ and a constant $r_0 > 0$ such that*

$$(2.5) \quad \mathbb{E}_{(x_0, \pi)}[e^{r_0 \tau_c}] < \infty$$

then (2.5) holds for π -a.e. initial values (x, π) .

Proof. Assume there exists a measurable set $A \subseteq E$ with $\pi(A) > 0$ such that

$$\mathbb{P}_{y, \pi}[e^{r_0 \tau_c}] = \infty$$

holds for any $y \in A$.

Let $x \in E$ be an arbitrary initial value. By the irreducibility of \mathbf{X} , there exists a time $T > 0$ such that the probability of $\mathcal{X}_T \in A$ is strictly positive. Denote the restricted measure of $P^T(x, \cdot)$ on A by λ_A . Now let $\mathcal{X}_0 = x$ and $\mathcal{Y}_0 \sim \pi$. Because (\mathbf{X}, \mathbf{Y}) is a coupling with independent components, the probability that \mathcal{X}_t and \mathcal{Y}_t remain being independent for $t = 0, 1, \dots, T$ is strictly positive. Since the Markov

process is non-atomic, so with probability 1, independent updates will not make \mathbf{X} and \mathbf{Y} couple. Hence, there exists a positive number $\delta > 0$ such that

$$\mathbb{P}[(\mathcal{X}_t, \mathcal{Y}_t) \in C] \geq \delta \cdot (\lambda_A \times \pi)(C)$$

for any measurable set $C \subseteq E \times E$.

Therefore, similar argument as in Lemma 2.2 gives

$$\mathbb{E}_{(x_0, \pi)}[e^{r_0 \tau_c}] \geq \delta e^{r_0 T} \cdot \mathbb{E}_{\lambda_A \times \pi}[e^{r_0 \tau_c}] = \infty.$$

This contradicts to (2.5). Hence, (2.5) must hold for π -a.e. initial values (x, π) . \square

It follows from Lemmata 2.2, 2.3, and 2.4 that for any coupling with independent components, the finiteness of $\mathbb{E}[e^{r_0 \tau_c}]$ can be generalized from one initial value to almost every initial values. In addition, by Markov inequality, the geometric ergodicity (and contraction) follows from the finiteness of $\mathbb{E}[e^{r_0 \tau_c}]$. However, the moment generating function is difficult to compute in practice, especially when r_0 is close to the critical value. Hence, we use the exponential tail $\mathbb{P}[\tau_c > t]$ instead. This is justified by the following Lemma.

Lemma 2.5. *For any two initial distributions μ and ν , if*

$$(2.6) \quad \limsup_{t \rightarrow \infty} \frac{1}{t} \log \mathbb{P}_{(\mu, \nu)}[\tau_c > t] \leq -r_0,$$

then for any $\epsilon > 0$, it holds that

$$\mathbb{E}_{(\mu, \nu)}[e^{(r_0 - \epsilon)\tau_c}] < \infty.$$

Proof. In fact, from equation (2.6) we have

$$\mathbb{P}_{(\mu, \nu)}[\tau_c > t] \leq e^{-(r_0 - \epsilon/2)t}, \quad \forall t \gg 1.$$

Thus, the tail of the integral $\mathbb{E}_{(\mu, \nu)}[e^{\tau_c(r_0 - \epsilon)}]$ is upper bounded by

$$\begin{aligned} & \int_{\omega: \tau_c(\omega) > M} e^{\tau_c(\omega)(r_0 - \epsilon)} d\mathbb{P}_{(\mu, \nu)}(\omega) \\ & \leq \sum_{i=M}^{\infty} e^{(i+1)(r_0 - \epsilon)} \mathbb{P}[\tau_c > i] \leq \sum_{i=M}^{\infty} e^{(i+1)(r_0 - \epsilon)} e^{-(r_0 - \epsilon/2)i} = e^{(r_0 - \epsilon)} \sum_{i=M}^{\infty} e^{-i\epsilon/2} \end{aligned}$$

which goes to zero as M goes to infinity.

Hence, $\mathbb{E}_{(\mu, \nu)}[e^{(r_0 - \epsilon)\tau_c}]$ must be finite. \square

Combine the above lemmata together, we have the following proposition.

Proposition 2.6. *Let (\mathbf{X}, \mathbf{Y}) be a coupling with independent components of a non-atomic Markov process.*

(i) If $\mathbb{P}_{x_0, y_0}[\tau_c > t]$ has an exponential decay rate $r > 0$ for an initial pair $(x_0, y_0) \in E \times E$, then for any $\epsilon > 0$, for $(\pi \times \pi)$ -a.e. initial pairs $(x, y) \in E \times E$, \mathbf{X} (or \mathbf{Y}) is geometrically contracting with rate $(r - \epsilon)$;

(ii) If $\mathbb{P}_{x_0, \pi}[\tau_c > t]$ admits an exponential decay rate $r > 0$ for an initial value $x_0 \in E$, then \mathbf{X} (or \mathbf{Y}) is geometrically ergodic with rate $(r - \epsilon)$.

2.3. An upper bound of geometric rate. The coupling inequality (2.2) usually only gives a lower bound of the geometric convergence/contraction rate. We argue that the upper bound of the geometric ergodicity can be estimated by using first passage times because of the existence of the optimal coupling.

For the sake of simplicity, we consider discrete-time Markov processes. Recall that for an optimal coupling, the equality in (2.2) holds. It has been shown that for any two mutually singular probabilities μ and ν on E , an optimal coupling with initial distribution $\mu \times \nu$ exists and was explicitly constructed in [17, 38].

Proposition 2.7. *Let $\mathbf{X} = \{X_t; t \in \mathbb{Z}_{\geq 0}\}$ and $\mathbf{Y} = \{Y_t; t \in \mathbb{Z}_{\geq 0}\}$ be two discrete-time Markov processes on E sharing the same transition probabilities with initial distributions δ_x and δ_y , respectively, where $x \neq y$. Assume that there exists a sequence of disjoint pairs of sets $\{(A_t, B_t)\}_{t=0}^{\infty}$ such that $x \in A_0, y \in B_0$. Let*

$$\eta_x = \min_{t>0} \{X_t \in A_t^c\}, \quad \eta_y = \min_{t>0} \{Y_t \in B_t^c\}.$$

Then if denote

$$\rho := \limsup_{t \rightarrow \infty} \frac{1}{t} \log (\mathbb{P}[\min\{\eta_x, \eta_y\} > t]),$$

the geometric rate of contraction is at most ρ .

Proof. Let $(\mathbf{X}, \mathbf{Y}) = \{(\mathcal{X}_t, \mathcal{Y}_t); t \in \mathbb{Z}_{\geq 0}\}$ be the optimal coupling of the Markov process with transition probabilities \mathcal{P} with initial distribution $\delta_x \times \delta_y$. Then $\{\mathcal{X}_t\}$ and $\{\mathcal{Y}_t\}$ are respective copies of $\{X_t\}$ and $\{Y_t\}$ such that

$$\|\delta_x P^t - \delta_y P^t\|_{TV} = 2\mathbb{P}[\tau_c > t].$$

Note at the coupling time τ_c we have $\mathcal{X}_{\tau_c} = \mathcal{Y}_{\tau_c}$. This means that before time τ_c , either \mathcal{X}_t has exited from A_t or \mathcal{Y}_t has exited from B_t . Note for any $t \geq 0$, \mathcal{X}_t (resp. \mathcal{Y}_t) has the same distribution as X_t (resp. Y_t). This completes the proof. \square

In Section 4.4, for a random perturbed circle map with a stable 2-periodic orbit, we give both an upper and a lower bound of the geometrically ergodic rate through the first exit time and the coupling time, respectively.

2.4. Deterministic dynamics and random perturbations. By a discrete- or continuous-time deterministic dynamical system, we mean an iterative mapping $f : E \rightarrow E$, or an ordinary differential equation (ODE)

$$(2.7) \quad dZ_t/dt = g(Z_t), \quad t \in \mathbb{R}$$

where g is a vector field on E which is locally Lipschitz continuous.

In this paper, we mainly focus on the Markov processes arising from random perturbations of deterministic dynamical systems. To be specific, we shall consider

(i) the random perturbation of a discrete-time dynamics $f : E \rightarrow E$ given by

$$(2.8) \quad X_{n+1} = f(X_n) + \zeta_n,$$

where $\{\zeta_n\}$ are independent random variables taking values in E which will be defined specifically in each particular situation;

(ii) the random perturbation of a continuous-time dynamics (2.7) given by a stochastic differential equation (SDE) on \mathbb{R}^k :

$$(2.9) \quad dX_t = g(X_t)dt + \sigma(X_t)dW_t,$$

where $\sigma(\cdot)$ is a $k \times k$ matrix-valued function, and W_t is a Wiener process on \mathbb{R}^k . Also, g and σ are assumed to be smooth enough to give a well-defined solution X_t for all $t > 0$.

Below we introduce basic notions of chaotic behaviors for deterministic dynamical systems. In section 4, we shall see that although geometric ergodicity usually holds when random perturbations are added, the rate can vary, as the random perturbation vanishes, in different ways if the unperturbed dynamics admits essentially distinct chaotic properties.

Periodicity, quasi-periodicity and ergodicity. For a deterministic dynamical system $\mathbf{Z} = \{Z_t; t \geq 0\}$ on the state space E , $z_0 \in E$ is called a periodic point if there exists $T > 0$ such that for any $t \geq 0$, $Z_{t+T}|_{z_0} = Z_t|_{z_0}$, where $\{Z_t|_{z_0}; t \geq 0\}$ denotes the solution of the system with initial value z_0 . The minimum of such T is called the period of z_0 . In particular, z_0 is called a fixed point if $T = 0$.

When the state space $E = \mathbb{T}^n (n \geq 1)$, a quasi-periodic solution for a deterministic dynamics on E is usually involved with several irrational independent frequencies. In particular, a map on \mathbb{S}^1 is said to be quasi-periodic if its derivative is a constant irrational number. Quasi-periodicity characterizes the kind of recurrent behavior that any positive-measured set can be visited infinitely often by a quasi-periodic orbit. This is in fact a special case of the Birkhoff ergodic theorem, which says that any positive-measured set can be visited repeatedly by orbits starting from almost every initial point, with average visiting times proportional to the set measure.

Hyperbolicity, uniform expanding and exponential (resp. polynomial) mixing. Both periodicity and quasi-periodicity only tell us the average recurrence behavior of the system. To develop more chaotic properties, we usually require some hyperbolic property of the system. Roughly speaking, a smooth deterministic system is said to be *uniform (resp. non-uniform) hyperbolic* if its tangent map admits both expanding and contracting directions with expanding and contracting rate being uniform (resp. non-uniform). By *uniform (resp. non-uniform) expanding* we mean that the tangent map only admits expanding directions with uniform (non-uniform) expanding rate. Uniform and non-uniform hyperbolicity or expanding dynamics always come with *mixing* behaviors in terms of decay of correlations of measure evolutions.

For deterministic dynamical systems, the decay of correlations looks at the system in a statistical way that how quickly the evolution of a certain observable converges to its expectation with respect to the invariant measure (if exists). A deterministic dynamics is said to be *exponential (resp. polynomial) mixing* if it has an exponential (resp. polynomial) rate of decay of correlations. It has been shown that uniform hyperbolic or expanding systems (e.g., the uniform expanding maps on \mathbb{S}^1) is exponential mixing, while for systems with non-uniform hyperbolicity, the exponential mixing property may be lost. A well-known example illustrating this is the almost

expanding map with only one neutral fixed point. This kind of system is known to be at most polynomial mixing (see [39]).

2.5. Numerical scheme of SDEs. In the real simulations, SDE (2.9) is numerically computed at discrete times. We usually choose a time step size $0 < h \ll 1$ and consider discrete-time trajectories $X_0, X_h, \dots, X_{nh}, \dots$. To avoid confusion and make notations consistent, we let $\mathbf{X} = \{X_t; t \in \mathbb{R}\}$ be the true trajectory of SDE (2.9), and $\bar{\mathbf{X}} = \{\bar{X}_t; t \in h\mathbb{Z}_{>0}\}$ be the trajectory of the numerical integrator. In addition, we denote $\mathbf{X}^h = \{X_n^h; n \in \mathbb{Z}_+\}$ as the time- h sample chain of \mathbf{X} such that $X_n^h = X_{nh}$, and $\bar{\mathbf{X}}^h = \{\bar{X}_n^h; n \in \mathbb{Z}_+\}$ as the time- h sample chain of $\bar{\mathbf{X}}$ with $\bar{X}_n^h = \bar{X}_{nh}$.

The most commonly used numerical schemes of stochastic differential equations is the Euler-Maruyama scheme

$$X_{(n+1)h} = X_{nh} + f(X_{nh})h + \sigma(X_{nh})\sqrt{h}N_n,$$

where $\{N_n\}$ are standard normal random variables independent for each n . Note that the time- h sample chain \bar{X}_n^h fits the setting of discrete-time random perturbed dynamics (2.8):

$$\bar{X}_{n+1}^h = \bar{X}_n^h + f(\bar{X}_n^h)h + \sigma(\bar{X}_n^h)\sqrt{h}N_n.$$

Euler-Maruyama method can be improved to the Milstein method. The 1D Milstein method reads

$$X_{(n+1)h} = X_{nh} + f(X_{nh})h + \sigma(X_{nh})\sqrt{h}N_n + \frac{1}{2}\sigma(X_{nh})\sigma'(X_{nh})(N_n^2 - 1)h.$$

In particular, in any dimensions, Euler-Maruyama method coincide with Milstein method if $\sigma(X_t)$ is a constant matrix.

Now we recall the strong and weak approximations defined in [29]. Let $T < \infty$ be a given finite time. If

$$\mathbb{E}[|\bar{X}_T - X_T|] \leq C(T)h^\gamma, \quad \gamma > 0$$

holds for each sufficiently small h , then we say that \bar{X}_t converges *strongly* to X_t with order γ . Let C_P^l denote the space of l times continuously differentiable functions with polynomial growth rate for the function itself and all partial derivatives up to order l . If for any test function $g \in C_P^{2(\gamma+1)}$ and any given finite time T , we have

$$|\mathbb{E}[g(\bar{X}_T)] - \mathbb{E}[g(X_T)]| \leq C(T)h^\gamma, \quad \gamma > 0,$$

then we say that $\bar{\mathbf{X}}$ converges to \mathbf{X} *weakly* with order γ .

It is well known that under suitable regularity conditions, Euler-Maruyama scheme has strong order of convergence 0.5 and weak order of convergence 1.0, and Milstein scheme has strong order of convergence 1.0 [29].

3. DESCRIPTION OF ALGORITHM

By numerically studying the coupling times, the main idea of this paper is to use the exponential tail of coupling time to estimate the geometric ergodicity of a stochastic process. Assume that numerically we obtain, for a pair of initial value (x_0, y_0) , that

$$\mathbb{P}_{x_0, y_0}[\tau_c > t] \approx Ce^{-rt}, \quad \forall t \gg 1,$$

then it follows from Proposition 2.6 that

$$\limsup_{t \rightarrow \infty} \frac{1}{t} \log(\|\delta_x P^t - \delta_y P^t\|_{TV}) < -r.$$

holds for almost every pair of initial values. The numerical verification of geometric ergodicity is similar, except y is replaced by samples from the invariant probability measure.

Since this paper mainly studies coupling times in a numerical way, we consider, for the sake of definiteness, the time-discrete Markov process as it fits the case of both random perturbations of an iterative mapping and the time- h sample chain of a numerical trajectory of an SDE.

3.1. Coupling methods. Consider a Markov coupling (\mathbf{X}, \mathbf{Y}) . In the theoretical proof, \mathcal{X}_t and \mathcal{Y}_t are coupled when $\mathcal{X}_t = \mathcal{Y}_t$, which is usually done by making both trajectories enter a “small set” which satisfies the minorization condition [36]. However, in the numerical estimation of coupling times, these couplings are not the most efficient ones. Instead, we will use a mixture of the following coupling methods to achieve numerical coupling efficiently.

Independent Coupling. Independent coupling means when running the coupling process (\mathbf{X}, \mathbf{Y}) , the noise terms in the two marginal processes \mathcal{X}_t and \mathcal{Y}_t are independent until they are coupled. In other words, we have

$$(\mathcal{X}_{t+1}, \mathcal{Y}_{t+1}) = (f(\mathcal{X}_t) + \zeta_t^1, f(\mathcal{Y}_t) + \zeta_t^2),$$

where ζ_t^1 and ζ_t^2 are independent random variables for each t . In the theoretical studies, independent coupling is frequently used together with renewal theory to prove different rates of convergence to the invariant probability measure. In this paper, the independent coupling is used to make the coupling process have some “independent components” so that Lemmata 2.3 and 2.4 are applicable.

Synchronous Coupling. Another commonly used way to couple two processes is the synchronous coupling. Contrary to the independent coupling for which randomness in the two stochastic trajectories are totally unrelated, in the synchronous coupling, we put the same randomness to both processes until they are coupled. Thus, we have

$$(\mathcal{X}_{t+1}, \mathcal{Y}_{t+1}) = (f(\mathcal{X}_t) + \zeta_t^1, f(\mathcal{Y}_t) + \zeta_t^2),$$

where $\zeta_t^1 = \zeta_t^2$ for $t < \tau_c$. The advantage of synchronous coupling is that if the deterministic part of the system already has enough stability so that it admits a random attractor, then \mathcal{X}_t will approach to \mathcal{Y}_t quickly when driven by the same noise term.

Reflection Coupling. When the state space has dimension bigger than 2, two Wiener processes will meet less often than the 1D case. This makes independent coupling less effective. Then the reflection coupling plays a role.

Take the Euler-Maruyama scheme of the SDE

$$dX_t = f(X_t)dt + \sigma dN_t$$

as an example, where σ is an invertible constant matrix. Recall that the Euler-Maruyama scheme of \bar{X}_t^h reads as

$$\bar{X}_{t+1}^h = \bar{X}_t^h + f(\bar{X}_t^h)h + \sigma\sqrt{h}N_t,$$

where N_t is a normal random variable with mean zero and covariance matrix Id. The reflection coupling means that we run the time- h chain $\bar{\mathcal{X}}_t^h$ as

$$\bar{\mathcal{X}}_{t+1}^h = \bar{\mathcal{X}}_t^h + f(\bar{\mathcal{X}}_t^h)h + \sigma\sqrt{h}W_t,$$

while run $\bar{\mathcal{Y}}_t^h$ as

$$\bar{\mathcal{Y}}_{t+1}^h = \bar{\mathcal{Y}}_t^h + f(\bar{\mathcal{Y}}_t^h)h + \sigma\sqrt{h}PN_t,$$

where $P = I - 2e_t e_t^\top$ is a projection matrix with

$$e_t = \frac{\sigma^{-1}(\bar{\mathcal{X}}_t^h - \bar{\mathcal{Y}}_t^h)}{\|\sigma^{-1}(\bar{\mathcal{X}}_t^h - \bar{\mathcal{Y}}_t^h)\|}.$$

In other words, the noise term is reflected against the hyperplane that orthogonally passes the midpoint of the line segment connecting $\bar{\mathcal{X}}_t^h$ and $\bar{\mathcal{Y}}_t^h$.

It has been proved that reflection coupling is optimal for Brownian motions [21, 35]. It also works well for many SDEs [7, 8, 14, 15, 35], including Langevin dynamics with degenerate noise [5, 16]. The reflection coupling introduced above is still applicable for some non-constant σ under suitable assumptions [35]. However, for general non-constant $\sigma(x)$, the “true reflection” is given by the Kendall-Cranston coupling with respect to the Riemannian matrix $\sigma^T(x)\sigma(x)$ [10, 20, 26], which is more difficult to implement numerically.

Maximal Coupling. When running numerical simulations, the above three couplings can only bring \mathcal{X}_t close to \mathcal{Y}_t . We still need a mechanism to make $\mathcal{X}_{t+1} = \mathcal{Y}_{t+1}$ with certain positive probability. The maximal coupling aims to achieve this. It is derived to couple two trajectories as much as possible at the next step, which is in fact modified from the now well-known Doeblin coupling [13]. We adopt the name “maximal coupling” from [23].

Assume that at certain time t , $(\mathcal{X}_t, \mathcal{Y}_t)$ takes the value $(x, y) \in E \times E$. Denote the probability measures associated with $f(x) + \zeta_t^1$ and $f(y) + \zeta_t^2$ by μ_x and μ_y , respectively. Let $\nu_{x,y}$ be the “minimum probability measure” of μ_x and μ_y such that

$$\nu_{x,y}(A) = \delta \min\{\mu_x(A), \mu_y(A)\},$$

where δ is a normalizer that makes $\nu_{x,y}$ a probability measure. Then the next step is sampled as

$$(\mathcal{X}_{t+1}, \mathcal{Y}_{t+1}) = (f(\mathcal{X}_t) + \zeta_t^1, f(\mathcal{Y}_t) + \zeta_t^2),$$

such that

- with probability $(1 - \delta)^2$,

$$\zeta_t^1 \sim \frac{1}{1 - \delta}(\mu_x - \delta\nu_{x,y}), \quad \zeta_t^2 \sim \frac{1}{1 - \delta}(\mu_y - \delta\nu_{x,y})$$

independently;

- with probability $\delta(1 - \delta)$,

$$\zeta_t^1 \sim \frac{1}{1 - \delta}(\mu_x - \delta\nu_{x,y}), \quad \zeta_t^2 \sim \nu_{x,y}$$

independently;

- with probability $\delta(1 - \delta)$,

$$\zeta_t^1 \sim \nu_{x,y}, \quad \zeta_t^2 \sim \frac{1}{1 - \delta}(\mu_y - \delta\nu_{x,y})$$

independently;

- with probability δ^2 ,

$$\zeta_t^1 = \zeta_t^2 \sim \nu_{x,y}.$$

In other words, \mathbf{X} and \mathbf{Y} are coupled if and only if the two samples fall into a “common future” simultaneously. We remark that the classical version of Doeblin coupling requires the two trajectories enter a certain predefined “small set” simultaneously. Then a construction called the Nummelin split guarantees them to be coupled with certain positive probability. When running numerical simulations, such a construction becomes unnecessary. We can couple them whenever the probability distributions of their next step have enough overlap.

3.2. Numerical Algorithm. We propose the following two numerical algorithms to estimate the exponential tail of the coupling time for the rate of geometric contraction and and geometric ergodicity, respectively. The input of **Algorithm 1** is a pair of initial points (x, y) , and the output is a lower bound of the geometric contraction rate of $\|\delta_x P^t - \delta_y P^t\|_{TV}$. **Algorithm 2** takes input of one point $x \in E$, and produces a lower bound of the convergence rate of $\|\delta_x P^t - \pi\|_{TV}$. In **Algorithm 2**, we need to sample from the invariant probability measure. This is done by choosing the initial value of \mathcal{Y}_0 from a long trajectory of X_t , such that \mathcal{Y}_0 is approximately sampled from the invariant distribution π .

Since the geometric ergodicity implies the geometric contraction, in practice, it is sufficient to only run **Algorithm 2** to detect the rate of geometric convergence/contraction.

It remains to discuss the implementation of the maximal coupling. If the probability density function of both \mathcal{X}_{t+1} and \mathcal{Y}_{t+1} can be explicitly given, denoted by $p^{(x)}(x)$ and $p^{(y)}(x)$ respectively, one can perform coupling by comparing these two probability density functions. The algorithm is described in **Algorithm 3**. It is similar to the implementation described in [23, 25]

Remark 3.1. As discussed in Section 2.2, the reflection or synchronous coupling does not give an irreducible process in general, and we use a mixture of independent coupling and reflection (or synchronous) coupling so that the coupling has “independent components”. To achieve this, at each step, we generate an i.i.d. Bernoulli

Algorithm 1 Estimate geometric rate of contraction

Input: Initial values $x, y \in E$
Output: A lower bound of geometric rate of contraction $r > 0$
Choose threshold $d > 0$
for $i = 1$ to N **do**
 $\tau_i = 0, t = 0, (\mathcal{X}_t, \mathcal{Y}_t) = (x, y)$
 Flag = 0
 while Flag = 0 **do**
 if $|\mathcal{X}_t - \mathcal{Y}_t| > d$ **then**
 Compute $(\mathcal{X}_{t+1}, \mathcal{Y}_{t+1})$ using reflection coupling, synchronous coupling,
or independent coupling
 $t \leftarrow t + 1$
 else
 Compute $(\mathcal{X}_{t+1}, \mathcal{Y}_{t+1})$ using maximal coupling
 if $\zeta_t^1 = \zeta_t^2 \sim \nu_{x,y}$ **then**
 Flag = 1
 $\tau_i = t$
 else
 $t \leftarrow t + 1$
 end if
 end if
 end while
end for
Use τ_1, \dots, τ_N to Compute $\mathbb{P}[\tau > t]$
Fit $\log \mathbb{P}[\tau > t]$ versus t by a linear function. Compute the slope $-r$.

random variable Γ with $\mathbb{P}[\Gamma = 1] = \beta > 0$, which is independent of everything else. The independent coupling is chosen whenever $\Gamma = 1$, and we use reflection (or synchronous) coupling for otherwise. It then follows from Lemmata 2.3 and 2.4 that the exponential tail of the coupling time can be generalized to almost every initial values.

In practice, for all examples we have tested and all couplings we have used, exponential tails starting from different initial values have the same rate. We believe that the requirement of independent components is only a technical limitation. Lemmata 2.3 and Lemma 2.4 should hold a very general class of irreducible Markov processes and couplings.

4. GEOMETRIC ERGODICITY OF TIME-DISCRETE STOCHASTIC DYNAMICS

It has long been observed that for qualitatively different deterministic dynamical systems, their small random perturbations also have qualitatively different asymptotic dynamics [33]. In this section, we perform numerical examples of random perturbations of four deterministic dynamics on \mathbb{S}^1 with qualitatively different chaotic behavior: (1) an expanding map with exponential mixing rate; (2) a circle map

Algorithm 2 Estimate convergence rate to π

Input: Initial values $x \in E$
Output: A lower bound of convergence rate $r > 0$ to π

Choose a threshold $d > 0$, another initial point $y \in E$, and a time step size H

Let $y_0 = y$
for $i = 1$ to N **do**

Let $X_0 = y_{i-1}$. Simulate X_t for time H
 $y_i \leftarrow X_H$
 $\tau_i = 0, t = 0, (\mathcal{X}_t, \mathcal{Y}_t) = (x, y_i)$

Flag = 0

while Flag = 0 **do**
if $|\mathcal{X}_t - \mathcal{Y}_t| > d$ **then**

Compute $(\mathcal{X}_{t+1}, \mathcal{Y}_{t+1})$ using reflection coupling, synchronous coupling, or independent coupling

 $t \leftarrow t + 1$
else

Compute $(\mathcal{X}_{t+1}, \mathcal{Y}_{t+1})$ using maximal coupling

if $\zeta_t^1 = \zeta_t^2 \sim \nu_{x,y}$ **then**

Flag = 1

 $\tau_i = t$
else
 $t \leftarrow t + 1$
end if
end if
end while
end for

Use τ_1, \dots, τ_N to Compute $\mathbb{P}[\tau > t]$

Fit $\log \mathbb{P}[\tau > t]$ versus t by a linear function. Compute the slope $-r$.

admitting a neutral fixed point and a polynomial mixing rate; (3) a circle map admitting quasi-periodic orbits on \mathbb{S}^1 ; (4) a circle map admitting a stable periodic orbit. We note that the chaotic behaviors of dynamics in (1) – (4) becomes weaker. For random perturbations of the above four deterministic dynamics, the rate of geometric convergence are compared under different magnitudes of noise. Qualitative different changes of the geometric convergence rates are observed among the above four examples as the noise vanishes. In general, when the noise is sufficiently small, as the underlying deterministic dynamic becomes more chaotic, the geometric convergence rate decreases in a slower way.

4.1. Smooth expanding circle maps. Consider a deterministic dynamics $Z_{n+1} = f(Z_n)$ given by the iterative mapping $f : \mathbb{S}^1 \rightarrow \mathbb{S}^1$:

$$f(x) = 2x + a \sin(2\pi x) \pmod{1}.$$

Algorithm 3 Maximal coupling**Input:** $(\mathcal{X}_t, \mathcal{Y}_t)$ **Output:** $(\mathcal{X}_{t+1}, \mathcal{Y}_{t+1})$, and τ_c if coupling is successful.Sample $(\mathcal{X}_{t+1}, \mathcal{Y}_{t+1})$ using independent couplingCompute probability density functions $p^{(x)}(x)$ and $p^{(y)}(x)$.

Let

$$r = \frac{\min\{p^{(x)}(\mathcal{X}_{t+1}), p^{(y)}(\mathcal{X}_{t+1})\}}{\max\{p^{(x)}(\mathcal{X}_{t+1}), p^{(y)}(\mathcal{X}_{t+1})\}} \times \frac{\min\{p^{(x)}(\mathcal{Y}_{t+1}), p^{(y)}(\mathcal{Y}_{t+1})\}}{\max\{p^{(x)}(\mathcal{Y}_{t+1}), p^{(y)}(\mathcal{Y}_{t+1})\}}$$

Draw u from uniform 0-1 distribution.**if** $u < r$ **then**

$$\mathcal{X}_{t+1} = \mathcal{Y}_{t+1}, \tau_c = t + 1$$

elseUse $(\mathcal{X}_{t+1}, \mathcal{Y}_{t+1})$ sampled before τ_c is still undetermined.**end if**

It is easy to see that for $a < 1/2\pi$, f is uniformly expanding. It is well known that the dynamical system $\mathbf{Z} = \{Z_n; n \in \mathbb{Z}_{\geq 0}\}$ admits an exponential mixing rate and an invariant probability measure with smooth density.

We consider a random perturbation of \mathbf{Z} through a Markov process \mathbf{X} given by

$$(4.1) \quad X_{n+1} = f(X_n) + \epsilon \zeta_n \pmod{1}$$

where $\{\zeta_n\}$ are i.i.d. standard normal random variables, and ϵ is the noise magnitude.

In our simulations, we run **Algorithm 2** with $N = 10^8$ samples and collect coupling times. The slope of exponential of the coupling time gives the rate of geometric ergodicity. Noise magnitudes ϵ are chosen to be 0.01, 0.02, 0.04, \dots , 0.12. The $\mathbb{P}[\tau_c > t]$ vs. t plots are demonstrated in log-linear plot in Figure 1. We can see that the coupling time has an exponential tail. The slope of the exponential tail vs. ϵ is also plotted in Figure 1 (lower right corner). The slope of exponential tail drops linearly with the strength of noise. This is expected because $\epsilon \zeta_t$ has a standard deviation ϵ . Hence, the distance between two trajectories need to be $O(\epsilon)$ in order to couple. If we assume that \mathbf{Z} is well-mixed, heuristically two trajectories should take $O(\epsilon^{-1})$ time to be $O(\epsilon)$ close to each other.

4.2. Circle map with neutral fixed point. The second example is a circle map with a neutral fixed point. Consider

$$f(x) = \begin{cases} x + 2^\alpha x^{1+\alpha}, & 0 \leq x \leq \frac{1}{2} \\ 2x - 1, & \frac{1}{2} < x < 1, \end{cases}$$

where $0 < \alpha < 1$ is a parameter. It is well known that the deterministic dynamical system $Z_{n+1} = f(Z_n)$ has a neutral fixed point at $x = 0$. As a result, the dynamical system $\mathbf{Z} = \{Z_n; n \in \mathbb{Z}_{\geq 0}\}$ has power-law mixing rate $n^{1-1/\alpha}$ [39].

Now we consider \mathbf{X} , the small random perturbation of \mathbf{Z} , which is given by

$$X_{n+1} = f(X_n) + \epsilon \zeta_n \pmod{1},$$

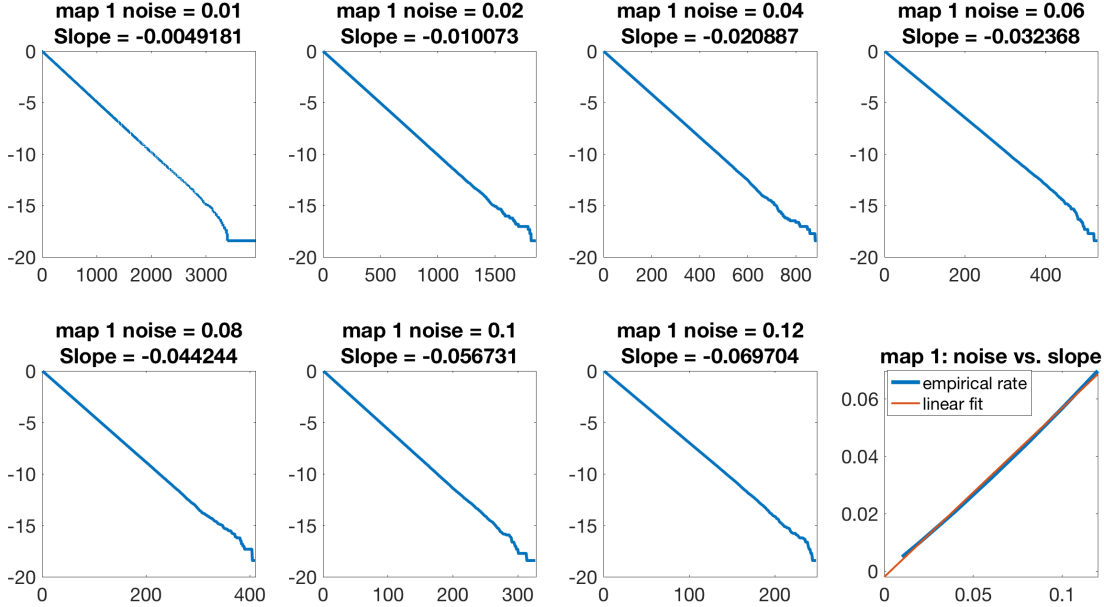


FIGURE 1. First 7 panels: $\mathbb{P}[\tau_c > t]$ vs. t with different noise terms. Lower right panel: exponential tail vs. ϵ and linear fit.

where $\{\zeta_n\}$ are i.i.d. standard normal random variables.

Still, we run **Algorithm 2** with $N = 10^8$ samples and collect coupling times to compute the rate of geometric ergodicity. Noise magnitudes ϵ are the same as before. The $\mathbb{P}[\tau_c > t]$ vs. t plots are demonstrate in log-linear plot in Figure 2. The coupling time still has a good exponential tail. The slope of the exponential tail vs. ϵ is also plotted in Figure 2 (lower right corner). In spite of slower mixing rate, the slope of exponential tail drops linearly with the strength of noise, which is same as the exponential mixing example. This is because the slow mixing of \mathbf{Z} is caused by a longer return time from very small neighborhood of the neutral fixed point. Very small noise is sufficient to “shake” trajectories away from the neutral fixed point and maintain a suitable mixing rate. Hence, the effect of slower-mixing rate can not be observed unless the noise term becomes extremely small. We refer [3, 4] for some recent theoretical results for similar maps with very small random perturbation.

4.3. Quasi-periodic map. The next example is the quasi-periodic map

$$f(x) = x + \sqrt{2} \pmod{1}.$$

It is easy to see that the orbit of $Z_{n+1} = f(Z_n)$ is quasi-periodic, which is ergodic but not mixing. Now we consider the Markov process \mathbf{X} that is given by

$$X_{n+1} = f(X_n) + \epsilon \zeta_n \pmod{1},$$

where $\{\zeta_n\}$ are i.i.d. standard normal random variables.

The rate of geometric ergodicity is computed by running **Algorithm 2** with $N = 10^8$ samples and collect coupling times. Noise magnitudes ϵ are same as before.

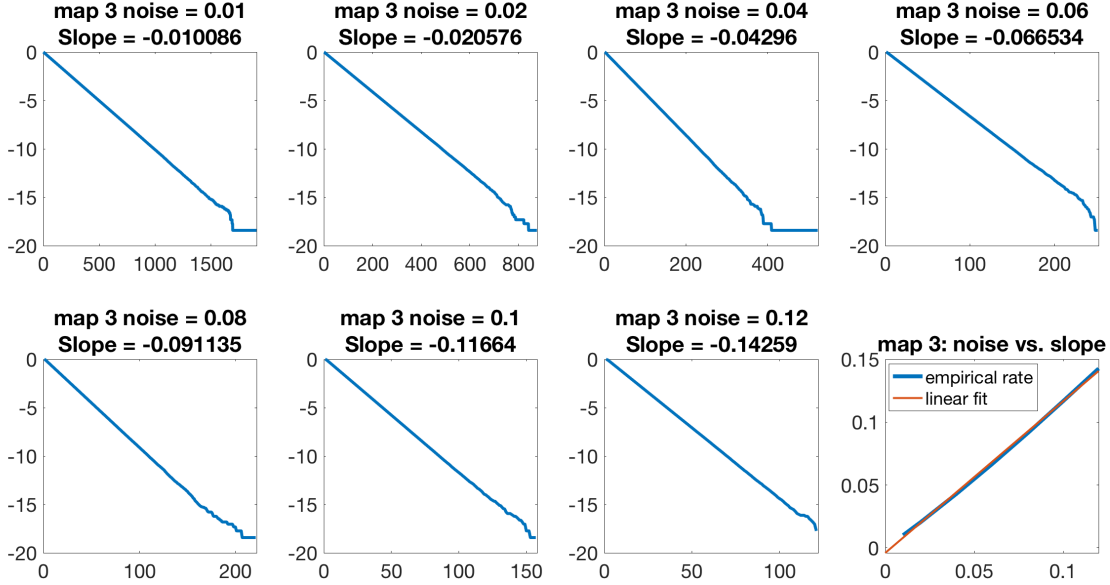


FIGURE 2. First 7 panels: $\mathbb{P}[\tau_c > t]$ vs. t with different noise terms. Lower right panel: exponential tail vs. ϵ and linear fit.

The $\mathbb{P}[\tau_c > t]$ vs. t plots are demonstrate in log-linear plot in Figure 3. Tails of the coupling time are still exponentials. The slope of the exponential tail vs. ϵ is also plotted in Figure 3 (lower right corner). Different from the previous two examples, in this example, the slope of exponential tail drops super-linearly with the strength of noise. We find that a cubic polynomial function can fit this slope vs. ϵ curve fairly well, as shown in Figure 3 lower right corner. The heuristic reason for the $O(\epsilon^3)$ slope is the following. Without mixing, the only force that brings two trajectories together is the diffusion, which takes $O(\epsilon^{-2})$ time to move $O(1)$ distance. Hence one expect two trajectories to be “well mixed” after $O(\epsilon^{-2})$ time. In addition they need to be $O(\epsilon)$ close to each other to couple. This brings the requiring total time needed to $O(\epsilon^{-3})$.

4.4. **Stable periodic orbit.** The last example is the Logistic map. Consider

$$f(x) = 3.2x(1 - x) \pmod{1}.$$

The deterministic dynamical system $Z_{n+1} = f(Z_n)$ admits a periodic orbit with period 2 that attracts all initial values on $(0, 1)$. The two values of this periodic orbit, P and Q , are approximately 0.7995 and 0.5130, respectively.

Now we consider the small random perturbation of $\mathbf{Z} = \{Z_n; n \in \mathbb{Z}_+\}$, which is a Markov process \mathbf{X} given by

$$X_{n+1} = f(X_n) + \epsilon \zeta_n \pmod{1},$$

where $\{\zeta_n\}$ are i.i.d. standard normal random variable.

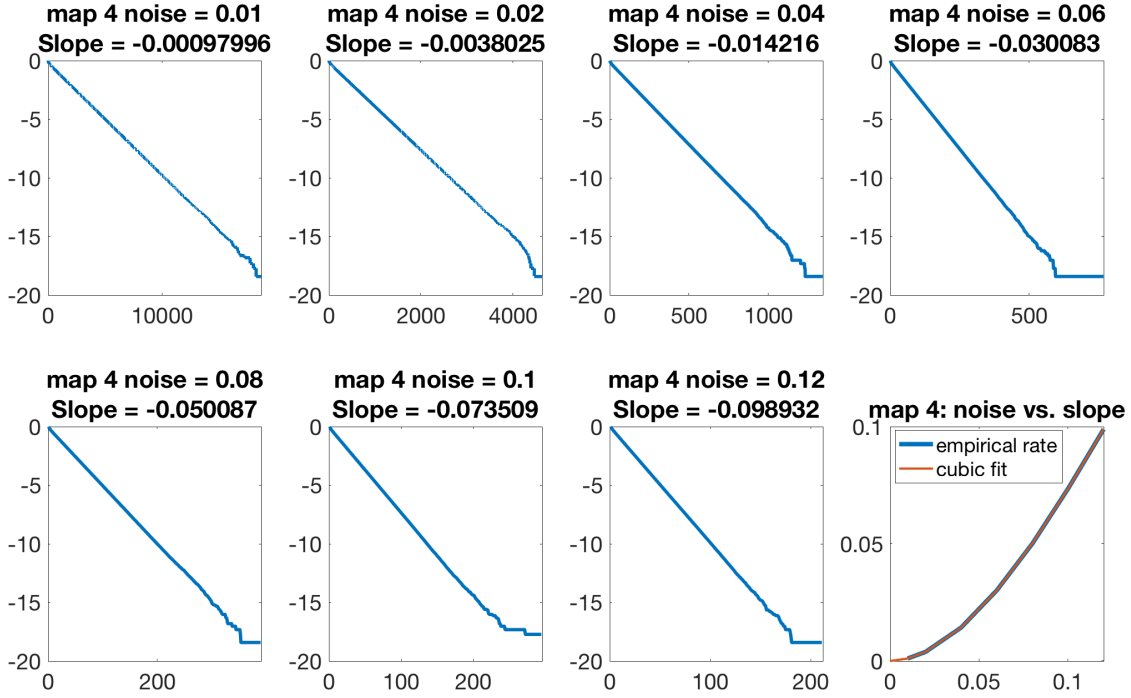


FIGURE 3. First 7 panels: $\mathbb{P}[\tau_c > t]$ vs. t with different noise terms.
Lower right panel: exponential tail vs. ϵ and linear fit.

We compute the rate of geometric ergodicity of \mathbf{X} with different noise magnitudes by running **Algorithm 2** with $N = 10^8$ trajectories. The parameter ϵ is chosen to be 0.02, 0.03, 0.04, 0.06, 0.08, 0.1, and 0.12, as coupling is extremely slow in this example if the noise is small. Slopes of exponential tails of the coupling times are demonstrated in Figure 4. We can see that when the noise is weak, the coupling becomes exponentially slow in this example (Figure 4 lower right corner). This is because the deterministic dynamics admits a stable periodic orbit. Two trajectories of \mathbf{Z} need to overcome the barrier between two distinct periodic orbits in order to meet. Large deviations theory tells us that this exit time is exponentially long.

In addition to the lower bound, we also compute the upper bound of the rate of geometric ergodicity through the first exit time. After some calculations, we find that the basin of attractions of the periodic sequence $PQPQPQ \cdots$ and $QPQPQP \cdots$ are

$$A = [0.110, 0.312] \cup [0.688, 0.890] \quad \text{and} \quad B = [0.313, 0.687],$$

respectively. So if a deterministic trajectory starts from A at $t = 0$, it converges to periodic orbit $PQPQPQ \cdots$, and if a deterministic trajectory starts from B at $t = 0$, it converges to the other periodic orbit $QPQPQP \cdots$. For each strength of ϵ computed above, we compute the first exit time η_{PQ} for (\mathbf{X}, \mathbf{Y}) starting from

(P, Q) such that

$$\eta_{PQ} = \min \left\{ \inf_{t \geq 0} \{t \mid \mathcal{X}_t \notin A, t \text{ even, or } \mathcal{X}_t \notin B, t \text{ odd} \}, \right. \\ \left. \inf_{t \geq 0} \{t \mid \mathcal{Y}_t \notin B, t \text{ even, or } \mathcal{Y}_t \notin A, t \text{ odd} \} \right\}$$

for 10^8 sample trajectories. The probability $\mathbb{P}[\eta_{PQ} > t]$ vs. t is also plotted in Figure 4. By Proposition 2.7, the first exit time gives an upper bound of the rate of geometric ergodicity. In other words, when ϵ is small, the upper bound of the rate of geometric ergodicity is also very small.

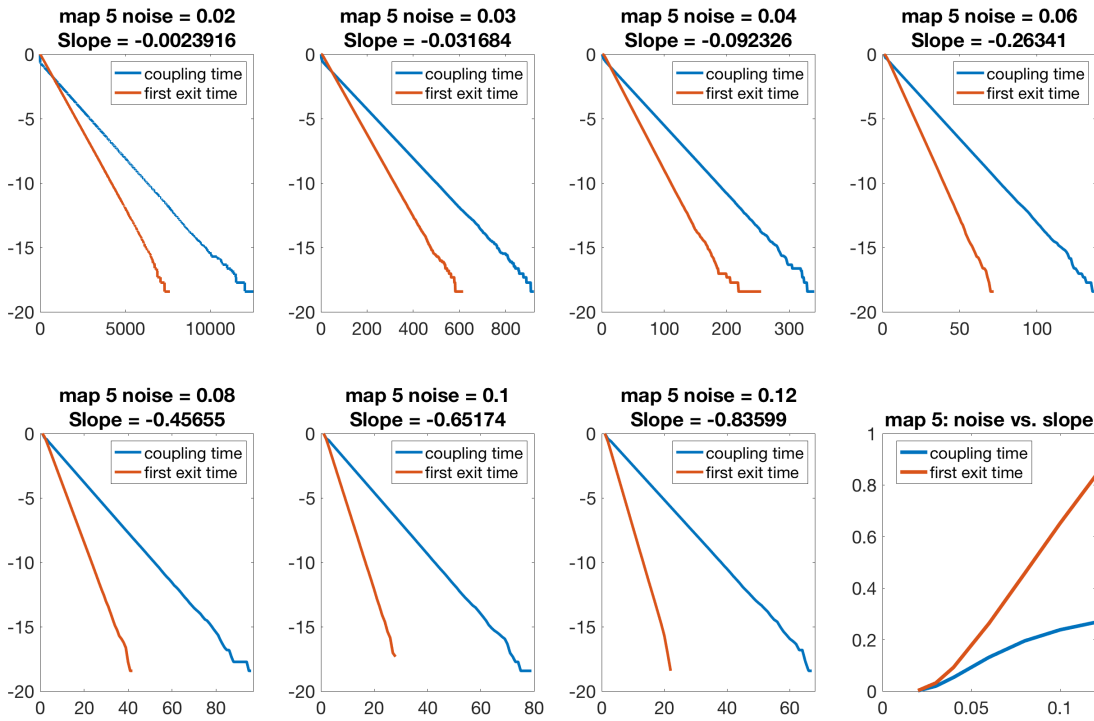


FIGURE 4. First 7 panels: Blue: $\mathbb{P}[\tau_c > t]$ vs. t with different noise terms. Red: $\mathbb{P}[\eta_{PQ} > t]$ vs. t with different noise terms. Lower right panel: exponential tail vs. ϵ for $\mathbb{P}[\tau_c > t]$ and $\mathbb{P}[\eta_{PQ} > t]$.

5. GEOMETRIC ERGODICITY OF STOCHASTIC DIFFERENTIAL EQUATIONS

5.1. Numerical and analytical coupling times. For SDEs, the first issue to address is the impact of numerical approximations. The independent coupling, synchronous coupling, and reflection coupling introduced in Section 3.1 can be applied to the continuous-time SDE (2.9) analogously. However, a numerical trajectory \tilde{X}_t

of the SDE is only an approximation of its true trajectory X_t . In addition, the mechanism of analytical couplings are different from the numerical ones. Two trajectories of X_t are coupled when they meet, without the need of triggering a maximal coupling one step earlier. Such difference makes a direct comparison of coupling times very difficult. Therefore, we need to apply the numerical coupling strategy in Section 3.1, i.e., triggering a maximal coupling when two trajectories are close to each other, to the time- h sample chain of the true SDE trajectory. This helps us to compare the coupling time under the same coupling mechanism. If the time- h sample chain \mathbf{X}^h is geometrically ergodic, then so is the original continuous-time process \mathbf{X} .

As in Section 2.5, for the SDE (2.9), we work on the time- h sample chains $\mathbf{X}^h = \{X_n^h; n \in \mathbb{Z}_{\geq 0}\}$ and $\bar{\mathbf{X}}^h = \{\bar{X}_n^h; n \in \mathbb{Z}_{\geq 0}\}$ with any small parameter $h > 0$. Applying the numerical coupling strategy described in **Algorithm 1** to \mathbf{X}^h , we will construct a coupling $(\mathbf{X}^h, \mathbf{Y}^h)$ of the time- h chain of (2.9), and show that the coupling probability of the numerical coupling $(\bar{\mathbf{X}}^h, \bar{\mathbf{Y}}^h) = \{(\bar{\mathcal{X}}_n^h, \bar{\mathcal{Y}}_n^h); n \in \mathbb{Z}_{\geq 0}\}$ converges to that of $(\mathbf{X}^h, \mathbf{Y}^h) = \{(\mathcal{X}_n^h, \mathcal{Y}_n^h); n \in \mathbb{Z}_{\geq 0}\}$. The coupling $(\mathbf{X}^h, \mathbf{Y}^h)$ is given as follows:

- (i) When the maximal coupling is not triggered, both $(\mathcal{X}_n^h, \mathcal{Y}_n^h)$ and $(\bar{\mathcal{X}}_n^h, \bar{\mathcal{Y}}_n^h)$ evolve according to the same coupling method (independent, reflection, or synchronous) for $n = 0, 1, \dots$;
- (ii) At each $t = nh, n \geq 0$, check the distance between \mathcal{X}_n^h and \mathcal{Y}_n^h , and trigger the maximal coupling if and only if $|\mathcal{X}_n^h - \mathcal{Y}_n^h| < d$, where d is the same threshold as in **Algorithm 1**;
- (iii) If the maximal coupling is triggered at $t = nh$, perform the maximal coupling with respect to the probability distribution of $\mathcal{X}_{(n+1)}^h$ and $\mathcal{Y}_{(n+1)}^h$, respectively.

(If at step (ii), we have $\mathcal{X}_n^h = \mathcal{Y}_n^h$, then $\tau_c = n$ and step (iii) will not be implemented. But for any strong Feller processes, this happens with zero probability.)

It is easy to see that $(\mathbf{X}^h, \mathbf{Y}^h)$ is a coupling of the time- h sample chain of the SDE (2.9). If in addition, we assume the following for $(\mathbf{X}^h, \mathbf{Y}^h)$ and $(\bar{\mathbf{X}}^h, \bar{\mathbf{Y}}^h)$, then the difference between $\mathbb{P}[\tau_c > n]$ and $\mathbb{P}[\bar{\tau}_c > n]$ can be estimated at all finite time $t = nh$.

- (a) The numerical scheme used in **Algorithm 1** is a strong approximation such that for any finite $t = nh$,

$$\mathbb{P}[|\bar{X}_i^h - X_i^h| > h^p] \leq C(t)h^{1+\beta}, \quad i = 0, 1, \dots, n$$

holds for some $p > 1/2$, $\beta > 0$, constant $C(t) > 0$, and all sufficiently small $h > 0$;

- (b) For each $z := x - y$, the probability density function of $Z := \mathcal{X}_1^h - \mathcal{Y}_1^h$ (resp. $\bar{Z} := \bar{\mathcal{X}}_1^h - \bar{\mathcal{Y}}_1^h$) given $\mathcal{X}_0^h = x, \mathcal{Y}_0^h = y$ (resp. $\bar{\mathcal{X}}_0^h = x, \bar{\mathcal{Y}}_0^h = y$), denoted by $p_z(Z)$ (resp. $p_z(\bar{Z})$), satisfies

$$C_b h^{-k/2} e^{-(Z-z)^\top S_b(Z-z)/h} \leq p_z(Z) \leq C_u h^{-k/2} e^{-(Z-z)^\top S_u(Z-z)/h},$$

(resp.

$$\bar{C}_b h^{-k/2} e^{-(\bar{Z}-z)^\top \bar{S}_b(\bar{Z}-z)/h} \leq p_z(\bar{Z}) \leq \bar{C}_u h^{-k/2} e^{-(\bar{Z}-z)^\top \bar{S}_u(\bar{Z}-z)/h}$$

-)
 for positive definite $k \times k$ matrices S_u, S_b (resp. \bar{S}_u, \bar{S}_b), and $O(1)$ constants C_u, C_b (resp. \bar{C}_u, \bar{C}_b);
- (c) The threshold $d = C\sqrt{h}$ for a constant $C > 0$;
- (d) The probability density function of X_1^h (resp. \bar{X}_1^h) conditioning on $X_0^h = x$ (resp. $\bar{X}_0^h = x$), denoted by f_x^h (resp. \bar{f}_x^h), changes continuously with h such that

$$\lim_{h \rightarrow 0} \|f_x^h - f_{x+h^\gamma}^h\|_{L^1} = 0 \quad (\text{resp. } \lim_{h \rightarrow 0} \|\bar{f}_x^h - \bar{f}_{x+h^\gamma}^h\|_{L^1} = 0)$$

for all $\gamma > 1/2$.

These assumptions essentially assume that (i) $\bar{\mathbf{X}}^h$ is a strong approximation of \mathbf{X}^h with good control of higher moments, and (ii) the probability density function of X_1^h given X_0^h (resp. \bar{X}_1^h given \bar{X}_0^h) is a good approximation of Gaussian function with variance $O(h)$.

Theorem 5.1. *Let τ_c and $\bar{\tau}_c$ be the coupling time of $(\mathbf{X}^h, \mathbf{Y}^h)$ and $(\bar{\mathbf{X}}^h, \bar{\mathbf{Y}}^h)$, respectively. Assume that assumptions (a)-(d) hold. Then for any finite time $t > 0$, we have*

$$\lim_{h \rightarrow 0} |\mathbb{P}[\tau_c > n_h] - \mathbb{P}[\bar{\tau}_c > n_h]| = 0,$$

where $n_h = \lfloor \frac{t}{h} \rfloor$.

Proof. We assume that two coupling processes $(\mathcal{X}_t, \mathcal{Y}_t)$ and $(\bar{\mathcal{X}}_t, \bar{\mathcal{Y}}_t)$ use the same Brownian motion of the true SDE trajectory to produce discrete random variables. This makes comparing distance between numerical trajectory and the true SDE trajectory possible.

For simplicity, let $t = n_h h$. Note that no coupling can occur when $n_h = 0$ or 1. Then we have

$$\begin{aligned} & |\mathbb{P}[\tau_c > n_h] - \mathbb{P}[\bar{\tau}_c > n_h]| = |\mathbb{P}[\tau_c \leq n_h] - \mathbb{P}[\bar{\tau}_c \leq n_h]| \\ (5.1) \quad & \leq \sum_{i=2}^{n_h} |\mathbb{P}[\tau_c = i] - \mathbb{P}[\bar{\tau}_c = i]|. \end{aligned}$$

Hence, we only need to show that $|\mathbb{P}[\tau_c = i] - \mathbb{P}[\bar{\tau}_c = i]|$ converges to 0 for each $2 \leq i \leq n_h$.

Note that if the coupling between $\bar{\mathcal{X}}_n^h$ and $\bar{\mathcal{Y}}_n^h$ occurs at step i , then at step $(i-1)$ the maximal coupling must be triggered. By the $O(h^p)$ strong approximation in assumption (a), with high probability, the maximal coupling between \mathcal{X}_n^h and \mathcal{Y}_n^h is triggered as well.

Let $\delta < (p - \frac{1}{2})/3$. For $2 \leq i \leq n_h$, we further split each term in the summation (5.1) as follows

$$\begin{aligned} & \mathbb{P}[\tau_c = i] - \mathbb{P}[\bar{\tau}_c = i] \\ = & (\mathbb{P}[\tau_c = i, d - h^{p-\delta} \leq |\mathcal{X}_{i-1}^h - \mathcal{Y}_{i-1}^h| \leq d] + \mathbb{P}[\tau_c = i, |\mathcal{X}_{i-1}^h - \mathcal{Y}_{i-1}^h| < d - h^{p-\delta}]) \\ & - (\mathbb{P}[\bar{\tau}_c = i, d - h^{p-\delta} \leq |\bar{\mathcal{X}}_{i-1}^h - \bar{\mathcal{Y}}_{i-1}^h| \leq d] + \mathbb{P}[\bar{\tau}_c = i, |\bar{\mathcal{X}}_{i-1}^h - \bar{\mathcal{Y}}_{i-1}^h| < d - h^{p-\delta}]). \end{aligned}$$

We first estimate $\mathbb{P}[\tau_c = i, d - h^{p-\delta} \leq |\mathcal{X}_{i-1}^h - \mathcal{Y}_{i-1}^h| \leq d]$ and $\mathbb{P}[\bar{\tau}_C = i, d - h^{p-\delta} \leq |\bar{\mathcal{X}}_{i-1}^h - \bar{\mathcal{Y}}_{i-1}^h| \leq d]$, which are the probability that the coupling process falls at the ‘‘edge’’ of the triggering area.

Conditioning on the value at step $(i - 2)$, we have

$$\begin{aligned} & \mathbb{P}[\tau_c = i, d - h^{p-\delta} \leq |\mathcal{X}_{i-1}^h - \mathcal{Y}_{i-1}^h| \leq d] \\ &= \int_{\mathbb{R}^k \times \mathbb{R}^k} \mathbb{P}[\tau_c = i, d - h^{p-\delta} \leq |\mathcal{X}_{i-1}^h - \mathcal{Y}_{i-1}^h| \leq d \mid \mathcal{X}_{i-2}^h = x, \mathcal{Y}_{i-2}^h = y] \mu_{i-2}(dx, dy) \\ &\leq \int_{\mathbb{R}^k \times \mathbb{R}^k} \mathbb{P}[d - h^{p-\delta} \leq |\mathcal{X}_{i-1}^h - \mathcal{Y}_{i-1}^h| \leq d \mid \mathcal{X}_{i-2}^h = x, \mathcal{Y}_{i-2}^h = y] \mu_{i-2}(dx, dy), \end{aligned}$$

where $\mu_{i-2}(dx, dy)$ is the joint probability distribution of $(\mathcal{X}_{i-2}^h, \mathcal{Y}_{i-2}^h)$.

By assumption (b), the probability density function of $(\mathcal{X}_{i-1}^h - \mathcal{Y}_{i-1}^h)$ is Gaussian-like. We have the following comparison of $\mathbb{P}[d - h^{p-\delta} \leq |\mathcal{X}_{i-1}^h - \mathcal{Y}_{i-1}^h| \leq d \mid \mathcal{X}_{i-2}^h = x, \mathcal{Y}_{i-2}^h = y]$ and $\mathbb{P}[|\mathcal{X}_{i-1}^h - \mathcal{Y}_{i-1}^h| \leq d \mid \mathcal{X}_{i-2}^h = x, \mathcal{Y}_{i-2}^h = y]$.

(i) If $|x - y| \leq -\delta \ln h \cdot h^{1/2}$, then since $d = O(h^{1/2})$, within the set $\{|\mathcal{X}_{i-1}^h - \mathcal{Y}_{i-1}^h| \leq d\}$, the maximal density of $(\mathcal{X}_{i-1}^h - \mathcal{Y}_{i-1}^h)$ is at most $O(h^{-\delta})$ times the minimal density of $(\mathcal{X}_{i-1}^h - \mathcal{Y}_{i-1}^h)$. Then in consideration that the Lebesgue measure of $\{d - h^{p-\delta} \leq |\mathcal{X}_{i-1}^h - \mathcal{Y}_{i-1}^h| \leq d\}$ is $O(h^{(k-1)/2+p-\delta})$, which is $O(h^{p-\frac{1}{2}-\delta})$ times the Lebesgue measure of $\{|\mathcal{X}_{i-1}^h - \mathcal{Y}_{i-1}^h| \leq d\}$, we have

$$\begin{aligned} & \mathbb{P}[d - h^{p-\delta} \leq |\mathcal{X}_{i-1}^h - \mathcal{Y}_{i-1}^h| \leq d \mid \mathcal{X}_{i-2}^h = x, \mathcal{Y}_{i-2}^h = y] \\ &\leq h^{p-\frac{1}{2}-2\delta} \mathbb{P}[|\mathcal{X}_{i-1}^h - \mathcal{Y}_{i-1}^h| \leq d \mid \mathcal{X}_{i-2}^h = x, \mathcal{Y}_{i-2}^h = y]. \end{aligned}$$

(ii) If $|x - y| > -\delta \ln h \cdot h^{1/2}$, then the probability density of $(\mathcal{X}_{i-1}^h - \mathcal{Y}_{i-1}^h)$ within the set $\{|\mathcal{X}_{i-1}^h - \mathcal{Y}_{i-1}^h| \leq d\}$ is less than $e^{-(\delta \ln h)^2} h^{-k/2}$, which converges to zero faster than h^r for any $r > 0$. Hence,

$$\begin{aligned} & \mathbb{P}[d - h^{p-\delta} \leq |\mathcal{X}_{i-1}^h - \mathcal{Y}_{i-1}^h| \leq d \mid \mathcal{X}_{i-2}^h = x, \mathcal{Y}_{i-2}^h = y] \\ &\leq h^{p-\frac{1}{2}-\delta+r} \mathbb{P}[|\mathcal{X}_{i-1}^h - \mathcal{Y}_{i-1}^h| \leq d \mid \mathcal{X}_{i-2}^h = x, \mathcal{Y}_{i-2}^h = y] \end{aligned}$$

Combining the above two cases, we have

$$\begin{aligned} & \mathbb{P}[d - h^{p-\delta} \leq |\mathcal{X}_{i-1}^h - \mathcal{Y}_{i-1}^h| \leq d \mid \mathcal{X}_{i-2}^h = x, \mathcal{Y}_{i-2}^h = y] \\ &\leq h^{p-\frac{1}{2}-2\delta} \mathbb{P}[|\mathcal{X}_{i-1}^h - \mathcal{Y}_{i-1}^h| \leq d \mid \mathcal{X}_{i-2}^h = x, \mathcal{Y}_{i-2}^h = y] \end{aligned}$$

Integrating over the initial conditions, we have

$$\mathbb{P}[d - h^{p-\delta} \leq |\mathcal{X}_{i-1}^h - \mathcal{Y}_{i-1}^h| \leq d] \leq O(h^{p-\frac{1}{2}-2\delta}) \mathbb{P}[|\mathcal{X}_{i-1}^h - \mathcal{Y}_{i-1}^h| \leq d].$$

By noting that the coupling probability conditioning on the event $\{|\mathcal{X}_{i-1}^h - \mathcal{Y}_{i-1}^h| \leq d\}$ is independent of h for all h sufficiently small, we have

$$\begin{aligned} & \mathbb{P}[\tau_c = i, d - h^{p-\delta} \leq |\mathcal{X}_{i-1}^h - \mathcal{Y}_{i-1}^h| \leq d] \\ &\leq O(h^{p-\frac{1}{2}-2\delta}) \cdot O(1) \cdot \mathbb{P}[\tau_c = i, |\mathcal{X}_{i-1}^h - \mathcal{Y}_{i-1}^h| \leq d] \\ &\leq O(h^{p-\frac{1}{2}-2\delta}) \mathbb{P}[\tau_c = i]. \end{aligned}$$

Analogously, we get the similar estimation for \bar{X}_i^h

$$\mathbb{P}[\bar{\tau}_c = i, d - h^{p-\delta} \leq |\bar{\mathcal{X}}_{i-1}^h - \bar{\mathcal{Y}}_{i-1}^h| \leq d] = O(h^{p-\frac{1}{2}-2\delta})\mathbb{P}[\bar{\tau}_c = i].$$

Now it remains to compare $\mathbb{P}[\tau_c = i, |\mathcal{X}_{i-1}^h - \mathcal{Y}_{i-1}^h| < d - h^{p-\delta}]$ and $\mathbb{P}[\bar{\tau}_c = i, |\bar{\mathcal{X}}_{i-1}^h - \bar{\mathcal{Y}}_{i-1}^h| < d - h^{p-\delta}]$.

For the sake of simplicity, define events

$$\begin{aligned} A_{i-1} &= \{|\mathcal{X}_{i-1}^h - \mathcal{Y}_{i-1}^h| < d - h^{p-\delta}, \tau_c > i - 1\}, \\ \bar{A}_{i-1} &= \{|\bar{\mathcal{X}}_{i-1}^h - \bar{\mathcal{Y}}_{i-1}^h| < d - h^{p-\delta}, \bar{\tau}_c > i - 1\}, \\ B_{i-1} &= \{|\bar{\mathcal{X}}_{i-1}^h - \mathcal{X}_{i-1}^h| \leq \frac{1}{2}h^{p-\delta}, |\bar{\mathcal{Y}}_{i-1}^h - \mathcal{Y}_{i-1}^h| \leq \frac{1}{2}h^{p-\delta}\}, \end{aligned}$$

and

$$\begin{aligned} C_{i-1} &= \{|\mathcal{X}_{i-1}^h - \mathcal{Y}_{i-1}^h| < d, |\bar{\mathcal{X}}_{i-1}^h - \bar{\mathcal{Y}}_{i-1}^h| < d, |\bar{\mathcal{X}}_{i-1}^h - \mathcal{X}_{i-1}^h| \leq \frac{1}{2}h^{p-\delta}, \\ &\quad |\bar{\mathcal{Y}}_{i-1}^h - \mathcal{Y}_{i-1}^h| \leq \frac{1}{2}h^{p-\delta}, \tau_c > i - 1, \bar{\tau}_c > i - 1\}. \end{aligned}$$

Then it holds that

$$\mathbb{P}[\tau_c = i, A_{i-1}] = \mathbb{P}[\tau_c = i, C_{i-1}] + \mathbb{P}[\tau_c = i, A_{i-1} \setminus C_{i-1}]$$

and

$$\mathbb{P}[\bar{\tau}_c = i, \bar{A}_{i-1}] = \mathbb{P}[\bar{\tau}_c = i, C_{i-1}] + \mathbb{P}[\bar{\tau}_c = i, \bar{A}_{i-1} \setminus C_{i-1}].$$

By noting that $A_{i-1} \cap B_{i-1} \subseteq C_{i-1}$ and $\bar{A}_{i-1} \cap B_{i-1} \subseteq C_{i-1}$, respectively, we have

$$\mathbb{P}[\tau_c = i, A_{i-1} \setminus C_{i-1}] \leq \mathbb{P}[\tau_c = i, B_{i-1}^c] \leq \mathbb{P}[B_{i-1}^c].$$

and

$$\mathbb{P}[\bar{\tau}_c = i, \bar{A}_{i-1} \setminus C_{i-1}] \leq \mathbb{P}[\bar{\tau}_c = i, B_{i-1}^c] \leq \mathbb{P}[B_{i-1}^c],$$

respectively. Hence,

$$\begin{aligned} &|\mathbb{P}[\tau_c = i, |\mathcal{X}_{i-1}^h - \mathcal{Y}_{i-1}^h| < d - h^{p-\delta}] - \mathbb{P}[\bar{\tau}_c = i, |\bar{\mathcal{X}}_{i-1}^h - \bar{\mathcal{Y}}_{i-1}^h| < d - h^{p-\delta}]| \\ &\leq |\mathbb{P}[\tau_c = i, C_{i-1}] - \mathbb{P}[\bar{\tau}_c = i, C_{i-1}]| + 2\mathbb{P}[B_{i-1}^c]. \end{aligned}$$

By the strong approximation assumption (a), we have

$$\mathbb{P}[B_{i-1}^c] \leq C(h)h^{1+\beta}$$

for some $\beta > 0$.

By the continuity assumption (d), we have

$$\begin{aligned} &|\mathbb{P}[\tau_c = i, C_{i-1}] - \mathbb{P}[\bar{\tau}_c = i, C_{i-1}]| \\ &= |\mathbb{P}[\tau_c = i|C_{i-1}] - \mathbb{P}[\bar{\tau}_c = i|C_{i-1}]|\mathbb{P}[C_{i-1}] \leq \epsilon(h)\mathbb{P}[C_{i-1}] \end{aligned}$$

for some $\epsilon(h)$ that converges to 0 as $h \rightarrow 0$. Still, as long as the maximal coupling is triggered, the coupling probability is in order $O(1)$ which is independent of all small h . Therefore,

$$|\mathbb{P}[\tau_c = i, C_{i-1}] - \mathbb{P}[\bar{\tau}_c = i, C_{i-1}]| \leq \epsilon(h)\mathbb{P}[\tau_c = i, C_{i-1}] \leq \epsilon(h)\mathbb{P}[\tau_c = i].$$

Now combine all estimations above, we have

$$\begin{aligned} & |\mathbb{P}[\tau_c = i] - \mathbb{P}[\bar{\tau}_c = i]| \\ & \leq 2C(t)h^{1+\beta} + \epsilon(h)\mathbb{P}[\tau_c = i] + O(h^{p-\frac{1}{2}-2\delta})(\mathbb{P}[\tau_c = i] + \mathbb{P}[\bar{\tau}_c = i]). \end{aligned}$$

Since

$$\sum_{i=2}^{n_h} \mathbb{P}[\tau_c = i] \leq 1 \quad , \quad \sum_{i=2}^{n_h} \mathbb{P}[\bar{\tau}_c = i] \leq 1 ,$$

and $n_h = O(\frac{1}{h})$, we have

$$\lim_{h \rightarrow 0} \sum_{i=2}^{n_h} |\mathbb{P}[\tau_c = i] - \mathbb{P}[\bar{\tau}_c = i]| = 0 .$$

This completes the proof. □

In summary, if an extrapolation of small h shows that the exponential tail of the coupling time of $(\bar{\mathbf{X}}^h, \bar{\mathbf{Y}}^h)$ is strictly bounded away from zero, then it follows from Theorem 5.1 that the numerical coupling gives a lower bound of the geometric convergence/contraction rate of the SDE (2.9).

5.2. Overdamping Langevin dynamics. The first SDE example is the overdamping Langevin dynamics. We consider

$$(5.2) \quad dX_t = -\nabla V(X_t) + \epsilon dW_t,$$

for some potential function $V(x)$. It is well known that equation (5.2) admits a unique invariant probability measure π_ϵ with probability density

$$\rho_\epsilon = \frac{1}{K} e^{-2V(X)/\epsilon^2} ,$$

where K is a normalizer. In addition, it is known that if V is strictly convex such that $\text{Hess}(V) - R\text{Id}_n$ is positive definite, then π_ϵ satisfies Logarithmic Sobolev inequality with constant $\epsilon^2 R/2$. Hence, the geometric convergence rate is at least R . (We refer [30, 2] for details.) Therefore, we can check our numerical rate of geometric ergodicity with the above analytical result.

Consider $n = 2$ and $V(x, y) = (x^2 + y^2)/2$. This potential function is strictly convex with Hessian matrix Id_2 . We run **Algorithm 2** for different time step sizes $h = 0.0005, 0.001, 0.0015, 0.002, 0.0025$ and 0.003 . The sample size is $N = 10^7$. To reach the optimal coupling rate, we only use reflection coupling until the maximal coupling is triggered. Exponential tails of coupling time with different time step sizes are compared in Figure 5 Left. In addition, we linearly extrapolate slopes of exponential tails in Figure 5 Right. Figure 5 Right shows that the numerical computed rate of geometric ergodicity is very close to the theoretical bound. In addition, smaller time step size gives higher rate of geometric ergodicity. By Theorem 5.1, these numerically computed rates of geometric ergodicity are trustworthy.

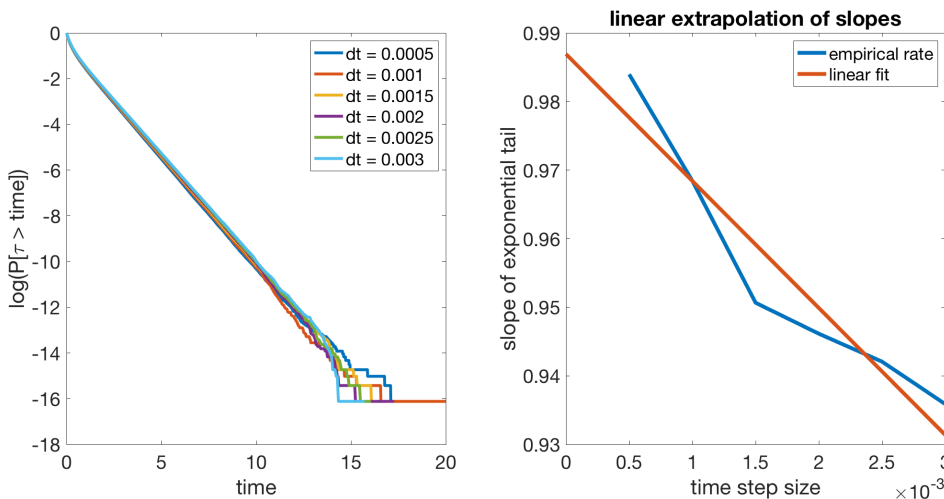


FIGURE 5. Left: Coupling time distribution of the overdamping Langevin dynamics under different time step sizes. Right: Comparison of exponential tails of coupling time with different time step sizes.

5.3. **Van der Pol oscillator.** The second SDE example is the Van der Pol oscillator with additive noise. We use this example to demonstrate the effect of slow-fast dynamics on the geometric ergodicity. Consider equation

$$(5.3) \quad \begin{aligned} dX_t &= (X_t - \frac{1}{3}X_t^3 - Y_t)dt + \epsilon dW_t^1 \\ dY_t &= \frac{1}{\mu}X_t dt + \epsilon dW_t^2 \end{aligned}$$

The deterministic part of equation (5.3) admits a limit cycle, as shown in Figure 6 Top Left. When $\mu \gg 1$, this system demonstrates slow-fast dynamics, called the relaxation oscillation. The solution will move slowly along left/right side of the limit cycle for a long time, and jump to the other side quickly after passing the “folding point”. See Figure 6 Top Right for x -trajectory versus time of the deterministic equation.

The slow-fast dynamics of the Van der Pol oscillator has been studied for decades. Today we use our methods to numerically study the spectral property of equation (5.3). The magnitude of noise is chosen to be $\epsilon = 0.3$, which is small comparing with the size of the oscillator. We run **Algorithm 2** with samples $N = 10^7$, time step size $h = 0.001$ and $\mu = 2, 4, 6, 8, 10, 12$. Before two trajectories are sufficiently close to each other, we use a mixture of independent coupling and reflection coupling. More precisely, at each step, with probability 0.05 we use the independent coupling, and the reflection coupling is used for otherwise. This makes the coupled process irreducible. We find that the resultant rate of the exponential tail is only slightly smaller than that of using pure reflection coupling. Exponential tails of coupling times with different μ are compared in Figure 6 Bottom Left. Note that this figure is cut off at probability $e^{-10} \approx 4.5 \times 10^{-5}$ and horizontally stretched in order to

demonstrate the difference between $\mu = 10$ plot and $\mu = 12$ plot. Slopes of these exponential tails versus different μ are compared in Figure 6 Bottom Right.

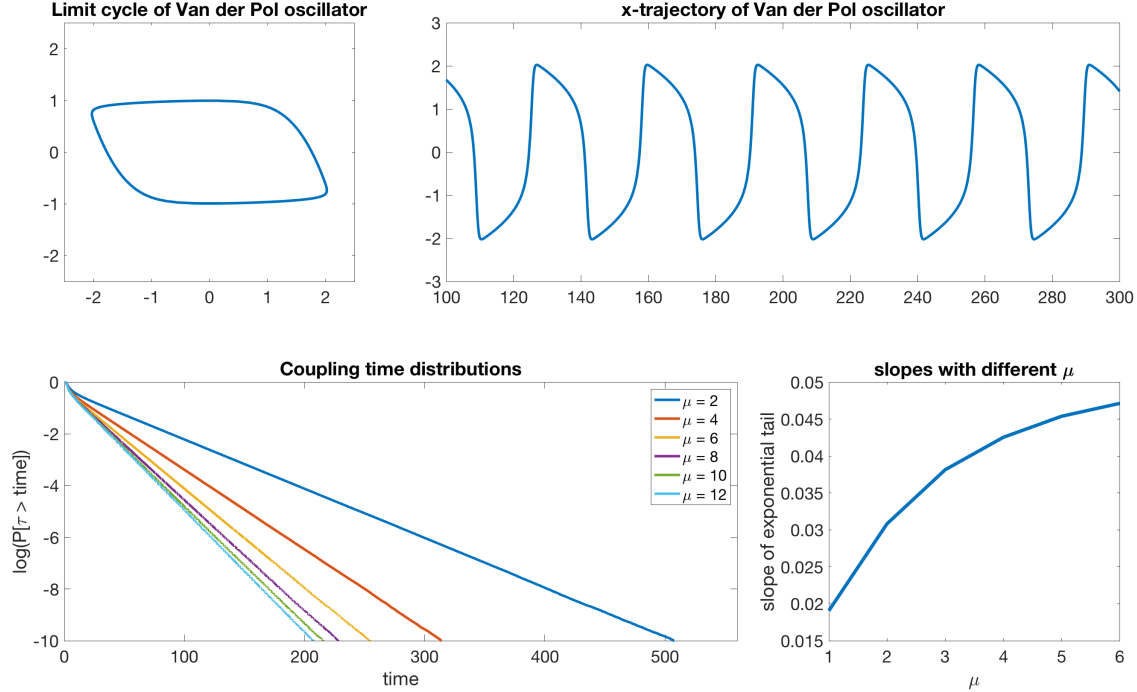


FIGURE 6. Top Left: limit cycle of the Van der Pol oscillator. Top Right: Deterministic trajectory of x -variable. Bottom Left: Exponential tails of coupling times with different values of parameter μ . Bottom Right: Slopes of exponential tails versus μ .

The rate of geometric ergodicity is small, which is expected because one trajectory needs to diffuse along the limit cycle to “chase” the other trajectory, which takes a considerable amount of time. In addition to this, one interesting observation is that the rate of geometric ergodicity increases significantly with the time separation scale μ . In other words, a larger time-scaling separation of slow-fast dynamics can make the law of equation (5.3) converges to its steady state distribution faster. To the best of our knowledge, this interesting phenomenon is not documented in previous studies. We believe the reason is that higher μ makes a trajectory move slower near the slow manifold, which can significantly increase the chance for two trajectories to “meet”.

5.4. SIR model with degenerate noise. In this subsection we use an SIR model with degenerate noise to demonstrate how our algorithm can be adapted for SDEs with degenerate diffusion terms. With degenerate diffusion, one step of the numerical algorithm does not produce a well defined probability density function on the state space. We need more than one step to implement the maximal coupling.

Consider an epidemic model in which the whole population is divided into three distinct classes S (susceptible class), I (infected class), and R (recovered class). An SIR model with population growth is given by

$$(5.4) \quad \begin{aligned} dS &= (\alpha - \beta SI - \mu S)dt \\ dI &= (\beta SI - (\mu + \rho + \gamma)I)dt \\ dR &= (\gamma I - \mu R)dt, \end{aligned}$$

where α is the population birth rate, μ is the disease-free death rate, ρ is the excess death rate for the infected class, γ is the recover rate for infected population, and β is the effective contact rate between susceptible class and infected class [11]. This model has been intensively studied. We refer [6, 28, 27] for a few representative references.

Now we assume that all the three classes are driven by the same random factor (such as temperature, humidity etc.). This gives an SDE with degenerate noise. Note that S and I in equation (5.4) are independent of R . So we consider the following SDE instead:

$$(5.5) \quad \begin{aligned} dS &= (\alpha - \beta SI - \mu S)dt + \sigma S dW_t \\ dI &= (\beta SI - (\mu + \rho + \gamma)I)dt + \sigma I dW_t, \end{aligned}$$

where the two dW_t terms are from the same Brownian motion. See Figure 7 Left for its trajectory in \mathbb{R}_+^2 .

In [11], several results about asymptotic dynamics of (5.5) are proved. Let

$$\lambda = \frac{\alpha\beta}{\mu} - (\mu + \rho + \gamma - \frac{\sigma^2}{2}).$$

If $\lambda > 0$, equation (5.5) admits a non-degenerate invariant probability measure on \mathbb{R}_+^2 . In addition, [11] shows that equation (5.5) approaches to its invariant probability measure faster than any polynomial of t . In this result, unable to obtain an exponential tail is mainly due to the technical limitation, as it is very challenging to construct an optimal Lyapunov function to control two different factors simultaneously. The Lyapunov function for equation (5.5) must take high values when S and I are either too large or too small.

We use **Algorithm 2** with adaptation of degenerate noise (which will be explained later) to examine the ergodicity of (5.5). The Model parameters are set as $\alpha = 7$, $\beta = 3$, $\mu = 1$, $\rho = 1$, $\gamma = 2$, and $\sigma = 1$, the same as the example used in [11]. The numerical algorithm we use is still Euler-Maruyama method with time step size $h = 0.001$. In **Algorithm 2**, we use synchronous coupling until two trajectories are sufficiently close to each other. Then we implement a two-step version of maximal coupling to check whether two trajectories can couple after more than two steps. The total sample size is 10^8 . The distribution of coupling time is demonstrated in Figure 7 Right. We can clearly see an exponential tail for $\mathbb{P}[\tau_c > t]$. Linear fitting gives a slope ≈ -0.53349 . Therefore, we conclude that equation (5.5) is indeed geometrically ergodic.

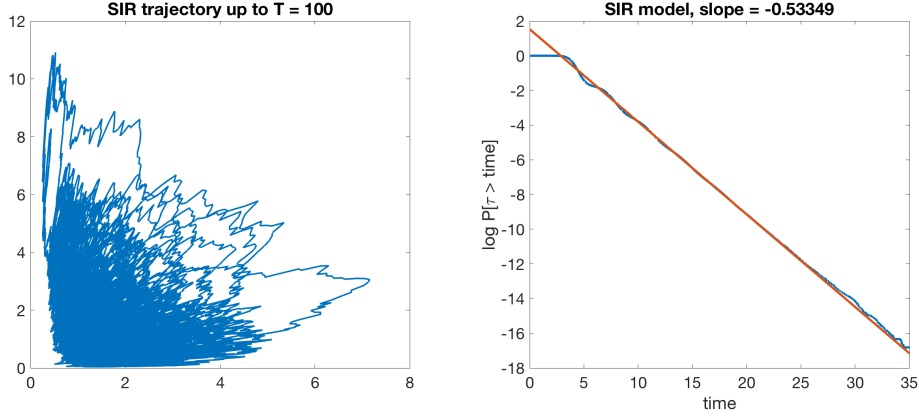


FIGURE 7. Left: Trajectory of equation (5.5) up to $T = 100$. Right: Coupling time distribution $\log(\mathbb{P}[\tau_c > t])$ vs. t and linear function fitting. Parameters are $\alpha = 7$, $\beta = 3$, $\mu = 1$, $\rho = 1$, $\gamma = 2$, and $\sigma = 1$.

We need to explain how to adapt **Algorithm 3** for the case of degenerate diffusion. This method also works for other similar problems with degenerate diffusion. It is not easy to explicitly estimate the probability density function after two steps of Euler-Maruyama method. (One exception is the Langevin dynamics because the derivative of position is a linear function of the velocity, which makes it possible to calculate an explicit probability density function. See the the first author's another paper [12].) Therefore, we need to study the transformation of probability density functions.

Let \bar{S}_n and \bar{I}_n be the approximate values of S_t^h and I_t^h at time $t = nh$ when running the Euler-Maruyama method. After one step of iteration, we have

$$\begin{aligned}\bar{S}_{n+1} &= \bar{S}_n + (\alpha - \beta\bar{S}_n\bar{I}_n - \mu\bar{S}_n)h + \sigma\bar{S}_n\sqrt{h}N_1 := \bar{S}_{n+1} + \sigma\bar{S}_n\sqrt{h}N_1, \\ \bar{I}_{n+1} &= \bar{I}_n + (\beta\bar{S}_n\bar{I}_n - (\mu + \rho + \gamma)\bar{I}_n)h + \sigma\bar{I}_n\sqrt{h}N_1 := \bar{I}_{n+1} + \sigma\bar{I}_n\sqrt{h}N_1,\end{aligned}$$

where N_1 is a standard normal random variable. After two steps, some calculations show that we have

$$(5.6) \quad \begin{aligned}\bar{S}_{n+2} &= \bar{S}_{n+1} + (\alpha - \beta\bar{S}_{n+1}\bar{I}_{n+1} - \mu\bar{S}_{n+1})h + R_S(N_1, N_2) \\ \bar{I}_{n+2} &= \bar{I}_{n+1} + (\beta\bar{S}_{n+1}\bar{I}_{n+1} - (\mu + \rho + \gamma)\bar{I}_{n+1})h + R_I(N_1, N_2),\end{aligned}$$

where N_1, N_2 are two independent standard normal random variables, transformations R_S and R_I are given by

$$(5.7) \quad \begin{aligned}R_S(N_1, N_2) &= [-\beta\sigma\bar{S}_n h^{3/2}\bar{I}_{n+1} - \beta\sigma\bar{I}_n h^{3/2}\bar{S}_{n+1} - \mu\sigma\bar{S}_n h^{3/2} + \sigma\bar{S}_n h^{1/2}]N_1 \\ &\quad + \sigma\bar{S}_{n+1} h^{1/2}N_2 - \beta\sigma^2\bar{S}_n\bar{I}_n h^2 N_1^2 + \sigma^2\bar{S}_n h N_1 N_2\end{aligned}$$

and

$$(5.8) \quad \begin{aligned}R_I(N_1, N_2) &= [\beta\sigma\bar{S}_n h^{3/2}\bar{I}_{n+1} + \beta\sigma\bar{I}_n h^{3/2}\bar{S}_{n+1} - (\mu + \rho + \gamma)\sigma\bar{I}_n h^{3/2} + \sigma\bar{I}_n h^{1/2}]N_1 \\ &\quad + \sigma\bar{I}_{n+1} h^{1/2}N_2 - \beta\sigma^2\bar{S}_n\bar{I}_n h^2 N_1^2 + \sigma^2\bar{I}_n h N_1 N_2,\end{aligned}$$

respectively. When h is sufficiently small, the transformation $(N_1, N_2) \mapsto (R_S, R_I)$ is close to a linear transformation because all quadratic coefficients are significantly smaller than the linear coefficients. Hence, we can treat this transformation as an invertible transformation when calculating the probability density function.

By elementary probability, it is easy to see that the joint probability density function $p(R_S, R_I)$ is given by

$$(5.9) \quad p(R_S, R_I) = |J|^{-1} p^{norm}(\bar{N}_1, \bar{N}_2),$$

where J is the Jacobian matrix of the transformation $(N_1, N_2) \mapsto (R_S, R_I)$, p^{norm} is the probability density function of the 2D standard normal random variable, and \bar{N}_1, \bar{N}_2 are values of random variables N_1 and N_2 that produces (R_S, R_I) .

Now let $\mathcal{X}_n^h = (\bar{S}_n^x, \bar{I}_n^x)$ and $\mathcal{Y}_n^h = (\bar{S}_n^y, \bar{I}_n^y)$ be two numerical trajectories that need to be coupled. Let p^x and p^y be the probability density functions of \mathcal{X}_{n+2}^h and \mathcal{Y}_{n+2}^h respectively. In **Algorithm 3**, we need to compute four probability densities, which are $p^x(\mathcal{X}_{n+2}^h)$, $p^x(\mathcal{Y}_{n+2}^h)$, $p^y(\mathcal{X}_{n+2}^h)$, and $p^y(\mathcal{Y}_{n+2}^h)$. Because we know the normal random variables N_1 and N_2 when sampling \mathcal{X}_{n+2}^h , $p^x(\mathcal{X}_{n+2}^h)$ is given by equation (5.9) directly. For $p^x(\mathcal{Y}_{n+2}^h)$, we need to calculate the “effective” (R_S^y, R_I^y) from equation (5.6) for \mathcal{X}_{n+2}^h , which is the “effective random terms” for \mathcal{X}_{n+2}^h to produce \mathcal{Y}_{n+2}^h . This is done by solving equations

$$\begin{aligned} \bar{S}_{n+2}^y &= \bar{S}_{n+1}^x + (\alpha - \beta \bar{S}_{n+1}^x \bar{I}_{n+1}^x - \mu \bar{S}_{n+1}^x)h + R_S^y(N_1^y, N_2^y) \\ \bar{I}_{n+2}^y &= \bar{I}_{n+1}^x + (\beta \bar{S}_{n+1}^x \bar{I}_{n+1}^x - (\mu + \rho + \gamma) \bar{I}_{n+1}^x)h + R_I^y(N_1^y, N_2^y). \end{aligned}$$

Then we need to solve (N_1^y, N_2^y) by numerically solving equation (5.7) and (5.8) for (R_S^y, R_I^y) . We use Newton’s method in our implementation, which converges after less than 5 steps. This gives the “effective normal random variables” for \mathcal{X}_{n+2}^h to produce \mathcal{Y}_{n+2}^h . The probability density function $p^x(\mathcal{Y}_{n+2}^h)$ is given by applying transformation (5.9) to the numerically solved (N_1^y, N_2^y) . The computation of $p^y(\mathcal{X}_{n+2}^h)$ and $p^y(\mathcal{Y}_{n+2}^h)$ are analogous.

5.5. Coupled stochastic FitzHugh-Nagumo model. The main advantage of the coupling method used in this paper is that it is relatively dimension-free. In contrast, approaches that rely on discretization of generator has significant difficulty in dealing with higher dimensional problems. In this subsection, we consider a very high dimensional example, in which many stochastically FitzHugh-Nagumo(FHN) oscillators are coupled. It is well known that FHN model is a nonlinear model that models the periodic evolution of membrane potential of a spiking neuron under external stimulation. For a single neuron, this model is a 2D dynamical system with additive noise

$$(5.10) \quad \begin{aligned} \mu du &= \left(u - \frac{1}{3}u^3 - v\right)dt + \sqrt{\mu}\sigma dW_t \\ dv &= (u + a)dt + \sigma dW_t, \end{aligned}$$

where u represents the membrane potential, and v is a recovery variable. When $a = 1.05$, the deterministic system admits a stable equilibrium with a small basin

of attraction. Intermittent limit cycles can be triggered by suitable random perturbations that is strong enough to drive the system out from the basin of attraction.

Consider 50 coupled equations (5.10) with both nearest-neighbor interaction and mean-field interaction. Similar as in [9], we let $v = \sqrt{\mu}v$ be the new recovery variable. This gives the coupled FHN oscillator

(5.11)

$$\begin{aligned} du_i &= \left(\frac{1}{\mu}u - \frac{1}{3\mu}u^3 - \frac{1}{\sqrt{\mu}}v + \frac{d_u}{\mu}(u_{i+1} + u_{i-1} - 2u_i) + \frac{w}{\mu}(\bar{u} - u_i) \right) dt + \frac{\sigma}{\sqrt{\mu}}dW_t \\ dv_i &= \left(\frac{1}{\sqrt{\mu}}u + \frac{a}{\sqrt{\mu}} \right) dt + \frac{\sigma}{\sqrt{\mu}}dW_t, \end{aligned}$$

for $i = 1, \dots, 50$, where d_u is the nearest-neighbor coupling strength, w is the mean field coupling strength, and

$$\bar{u} = \frac{1}{50} \sum_{i=1}^{50} u_i$$

is the mean membrane potential. In addition, we set $u_0 = u_{50}$ and $u_{51} = u_1$. Hence, the 50 neurons are connected as a ring. We would like to use this example to demonstrate the ability of our algorithm when dealing with high dimensional problem. The connection between ergodicity and degree of synchrony will also be discussed.

In our simulations, we choose parameters $w = 0.4$, $\mu = 0.05$, and $\sigma = 0.6$. These parameters are similar as those used in [9]. The main control parameter is du . Higher du means stronger nearest-neighbor coupling, which gives a more synchronized dynamics. See Figure 8 panel 1 to 5 for the time evolution of membrane potential with different du . We can see that higher du makes membrane potentials of 50 neurons evolve more coherently.

The numerical scheme in our simulation is the Euler-Maruyama scheme with $h = 0.001$. We run **Algorithm 2** with 10^6 samples for $du = 0, 0.1, 0.3, 0.5$, and 1 to compute exponential tails of the coupling time. See Figure 8 panel 6 for a comparison of coupling time distributions. We find that higher du gives a longer coupling time, and hence a lower rate of geometric ergodicity. Heuristically, this phenomenon is caused by the phase lock. In the presence of strong synchronization, the trajectory is attracted to the neighborhood of a high dimensional limit cycle and follows it as time evolves. When running the coupled process, two independent trajectories can be attracted to difference phases of this limit cycle. If this happen, it will take longer time for these two trajectories to couple, as one trajectory needs to diffuse by itself to “chase” the other trajectory through this limit cycle.

6. CONCLUSION AND FURTHER DISCUSSIONS

Geometric ergodicity is an important property of a stochastic process with infinitesimal generator. It measures the mixing effect given by a combination of the underlying deterministic dynamics and the random perturbations. In this paper, based on the coupling technique, we propose a probabilistic method to numerically compute the rate of geometric ergodicity. Some straightforward arguments show

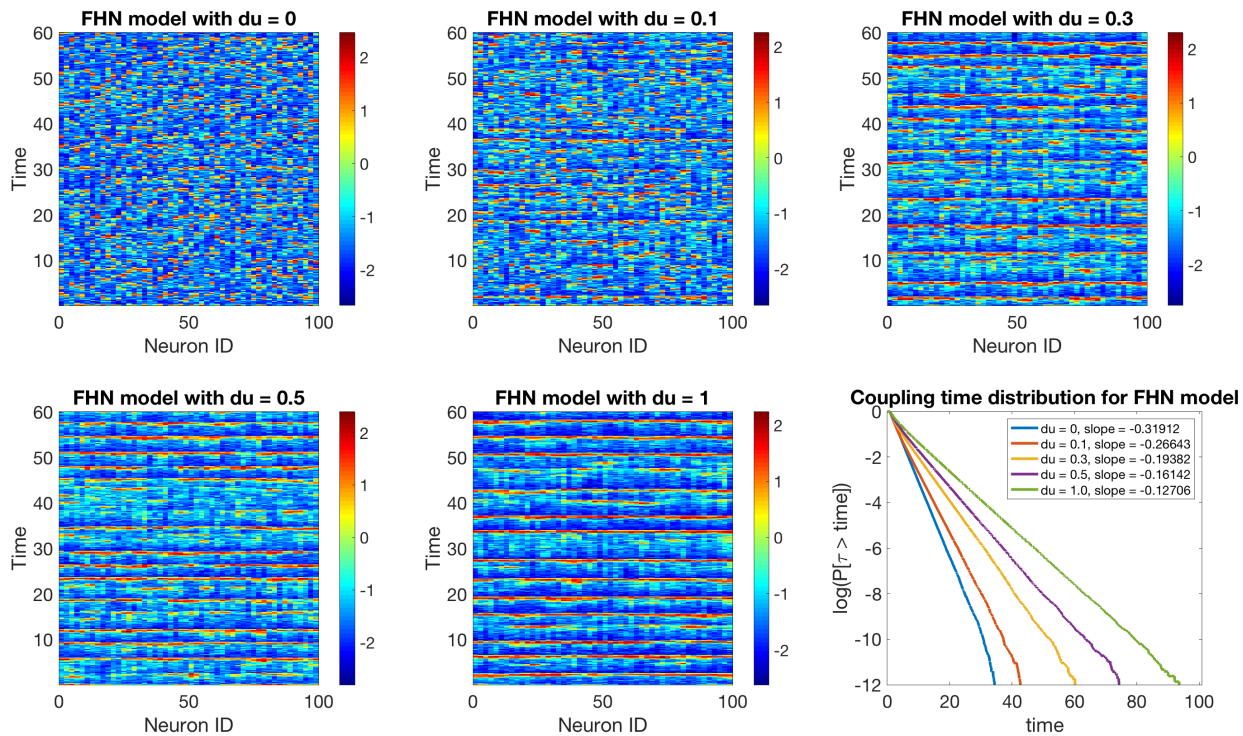


FIGURE 8. Panel I-V: Time evolutions of membrane potential of 50 coupled neurons in FHN model. Coupling strength du takes value 0, 0.1, 0.3, 0.5, and 1 in five figures. Different color means different membrane potential (See the color bar). X-axis: Neuron ID. Y-axis: Time. Panel VI: exponential tails of FHN model with five different du values.

that the lower bound of the rate can be estimated by computing the exponential tail of the coupling time. In addition, we find that the upper bound of the geometric convergence rate can be estimated by computing the first exit time with respect to a pair of disjoint sets. Compared with traditional method that looks for eigenvalues of discretized infinitesimal generator, our method is relatively dimension-free. It works well when the dimension of the phase space becomes too high for grid-based method.

As numerical examples, we study several deterministic dynamical systems with additive noise perturbations. One interesting finding is that the coupling time distribution under different magnitudes of noise terms can provide a lot of information about the deterministic dynamics. As demonstrated in Section 4, randomly perturbed dynamical systems has different convergence rate vs. noise curves when their underlying deterministic dynamics admits different degrees of chaos. In other words, coupling time provides some data-driven inference of the underlying deterministic dynamics. Since the coupling method is relatively dimension-free, we expect

this approach can be used to characterize some high-dimensional deterministic dynamical systems, such as gradient flows of high-dimensional potential functions. We plan to further explore along this direction in our future work.

Despite the success of the many examples, the coupling method has its own limitations. There are some known results about coupling with degenerate noise, such as coupling for the Langevin dynamics [16] or the Hamiltonian Monte Carlo method [5]. However, when the noise is highly degenerate, it becomes difficult to design an effective coupling scheme. In addition, with degenerate noise, the maximal coupling of numerical updates becomes significantly more difficult, as one needs to compute the probability density function of several consecutive updates in order to get a non-degenerate probability density function. As shown in Section 5.4, even the implementation of a relatively simple 2D example has some nontrivial overhead. At each step, one needs to run a nonlinear equation solver twice to check the probability of coupling. In this situation, a “weaker” approach which is based on numerical return time and analytical minorization condition works better. See the first author’s earlier paper [32] for reference. The method in [32] can numerically check the qualitative rate of ergodicity (geometric or sub-geometric), although in general it does not give a useful bound of rate of geometric ergodicity. The first author is currently writing a separate paper to extend the method in [32] to the case of SDEs with highly degenerate noise terms.

REFERENCES

- [1] David Aldous, *Random walks on finite groups and rapidly mixing Markov chains*, Séminaire de Probabilités XVII 1981/82, Springer, 1983, pp. 243–297.
- [2] Dominique Bakry and Michel Émery, *Diffusions hypercontractives*, Séminaire de Probabilités XIX 1983/84, Springer, 1985, pp. 177–206.
- [3] Alex Blumenthal, Jinxin Xue, and Lai-Sang Young, *Lyapunov exponents for random perturbations of some area-preserving maps including the standard map*, Annals of Mathematics (2017), 285–310.
- [4] ———, *Lyapunov exponents and correlation decay for random perturbations of some prototypical 2D maps*, Communications in Mathematical Physics **359** (2018), no. 1, 347–373.
- [5] Nawaf Bou-Rabee, Andreas Eberle, and Raphael Zimmer, *Coupling and convergence for Hamiltonian Monte Carlo*, arXiv preprint arXiv:1805.00452 (2018).
- [6] Vincenzo Capasso, *Mathematical structures of epidemic systems*, vol. 88, Springer, 1993.
- [7] Mu-Fa Chen and Feng-Yu Wang, *Estimation of spectral gap for elliptic operators*, Transactions of the American Mathematical Society **349** (1997), no. 3, 1239–1267.
- [8] Mufa Chen, *Estimation of spectral gap for Markov chains*, Acta Mathematica Sinica **12** (1996), no. 4, 337–360.
- [9] Nan Chen, Andrew J Majda, and Xin T Tong, *Spatial localization for nonlinear dynamical stochastic models for excitable media*, arXiv preprint arXiv:1901.07318 (2019).
- [10] Michael Cranston, *Gradient estimates on manifolds using coupling*, Journal of Functional Analysis **99** (1991), no. 1, 110–124.
- [11] Nguyen Thanh Dieu, Dang Hai Nguyen, Nguyen Huu Du, and George G Yin, *Classification of asymptotic behavior in a stochastic SIR model*, SIAM Journal on Applied Dynamical Systems **15** (2016), no. 2, 1062–1084.
- [12] Matthew Dobson, Jiayu Zhai, and Yao Li, *Using coupling methods to estimate sample quality for stochastic differential equations*, arXiv preprint arXiv:1912.10339 (2019).

- [13] Wolfgang Doeblin, *Exposé de la théorie des chaînes simples constantes de Markov á un nombre fini d'états*, Mathématique de l'Union Interbalkanique **2** (1938), no. 77-105, 78–80.
- [14] Andreas Eberle, *Reflection coupling and Wasserstein contractivity without convexity*, Comptes Rendus Mathématique **349** (2011), no. 19-20, 1101–1104.
- [15] ———, *Reflection couplings and contraction rates for diffusions*, Probability theory and related fields **166** (2016), no. 3-4, 851–886.
- [16] Andreas Eberle, Arnaud Guillin, Raphael Zimmer, et al., *Couplings and quantitative contraction rates for Langevin dynamics*, The Annals of Probability **47** (2019), no. 4, 1982–2010.
- [17] David Griffeath, *A maximal coupling for Markov chains*, Probability Theory and Related Fields **31** (1975), no. 2, 95–106.
- [18] Martin Hairer, *Convergence of Markov processes*, Lecture notes (2010).
- [19] Martin Hairer and Jonathan C Mattingly, *Yet another look at Harris ergodic theorem for Markov chains*, Seminar on Stochastic Analysis, Random Fields and Applications VI, Springer, 2011, pp. 109–117.
- [20] Elton P Hsu, *Stochastic analysis on manifolds*, vol. 38, American Mathematical Soc., 2002.
- [21] Elton P Hsu and Karl-Theodor Sturm, *Maximal coupling of Euclidean Brownian motions*, Communications in Mathematics and Statistics **1** (2013), no. 1, 93–104.
- [22] Alessandra Iacubucci, Stefano Olla, and Gabriel Stoltz, *Convergence rates for nonequilibrium Langevin dynamics*, Annales mathématiques du Québec **43** (2019), no. 1, 73–98.
- [23] Pierre E Jacob, John O'Leary, and Yves F Atchadé, *Unbiased Markov chain Monte Carlo with couplings*, arXiv preprint arXiv:1708.03625 (2017).
- [24] James E Johndrow and Jonathan C Mattingly, *Error bounds for approximations of Markov chains used in Bayesian sampling*, arXiv preprint arXiv:1711.05382 (2017).
- [25] Valen E Johnson, *A coupling-regeneration scheme for diagnosing convergence in Markov chain Monte Carlo algorithms*, Journal of the American Statistical Association **93** (1998), no. 441, 238–248.
- [26] Wilfrid S Kendall, *Coupled Brownian motions and partial domain monotonicity for the Neumann heat kernel*, Journal of Functional Analysis **86** (1989), no. 2, 226–236.
- [27] William O Kermack and McKendrick G Anderson, *Contributions to the mathematical theory of epidemics—I. 1927.*, Bulletin of mathematical biology **53** (1991), no. 1-2, 33.
- [28] William Ogilvy Kermack and Anderson G McKendrick, *Contributions to the mathematical theory of epidemics. II. The problem of endemicity*, Proceedings of the Royal Society of London. Series A, containing papers of a mathematical and physical character **138** (1932), no. 834, 55–83.
- [29] Peter E Kloeden and Eckhard Platen, *Numerical solution of stochastic differential equations*, vol. 23, Springer Science & Business Media, 2013.
- [30] Tony Lelièvre and Gabriel Stoltz, *Partial differential equations and stochastic methods in molecular dynamics*, Acta Numerica **25** (2016), 681–880.
- [31] Yao Li, *On the stochastic behaviors of locally confined particle systems*, Chaos: An Interdisciplinary Journal of Nonlinear Science **25** (2015), no. 7, 073121.
- [32] Yao Li and Hui Xu, *Numerical simulation of polynomial-speed convergence phenomenon*, Journal of Statistical Physics **169** (2017), no. 4, 697–729.
- [33] Kevin K Lin, *Convergence of invariant densities in the small-noise limit*, Nonlinearity **18** (2004), no. 2, 659–683.
- [34] Torgny Lindvall, *Lectures on the coupling method*, Courier Corporation, 2002.
- [35] Torgny Lindvall, L Cris G Rogers, et al., *Coupling of multidimensional diffusions by reflection*, The Annals of Probability **14** (1986), no. 3, 860–872.
- [36] Sean P Meyn and Richard L Tweedie, *Markov chains and stochastic stability*, Springer Science & Business Media, 2012.
- [37] Alexander Y Mitrophanov, *Sensitivity and convergence of uniformly ergodic Markov chains*, Journal of Applied Probability **42** (2005), no. 4, 1003–1014.

- [38] James W Pitman, *On coupling of Markov chains*, Probability Theory and Related Fields **35** (1976), no. 4, 315–322.
- [39] Lai-Sang Young, *Recurrence times and rates of mixing*, Israel Journal of Mathematics **110** (1999), no. 1, 153–188.

YAO LI: DEPARTMENT OF MATHEMATICS AND STATISTICS, UNIVERSITY OF MASSACHUSETTS
AMHERST, AMHERST, MA, 01002, USA

E-mail address: `yaoli@math.umass.edu`

SHIROU WANG: DEPARTMENT OF MATHEMATICAL & STATISTICAL SCIENCES, UNIVERSITY
OF ALBERTA, EDMONTON, ALBERTA, CANADA T6G2G1

E-mail address: `shirou@ualberta.ca`